Managed Aquifer Recharge in fractured crystalline rock aquifers: impact of horizontal preferential flow on recharge dynamics

Madeleine Nicolas [a,b †], Olivier Bour [b], Adrien Selles [a], Benoit Dewandel [c], Vincent Bailly-Comte [c], Subash Chandra [d], Shakeel Ahmed [d], Jean-Christophe Maréchal[c]

[a] *BRGM, Univ Montpellier, Indo-French Center for Groundwater Research, Uppal Road, 500007 Hyderabad, India*

[b] *Univ Rennes, CNRS, Géosciences Rennes - UMR 6118, F-35000 Rennes, France*

[c] *BRGM, Univ Montpellier, 34000 Montpellier, France*

[d] CSIR-*National Geophysical Research Institute, Indo-French Center for Groundwater Research, Uppal Road, 500007 Hyderabad, India*

Abstract

To overcome water scarcity issues, Managed Aquifer Recharge (MAR) structures are currently developed in many parts of the world, including poorly permeable terrain like weathered crystalline rocks. In such geological context, characterized by relatively limited groundwater storage mainly associated with fractures located at the interface between the upper weathered layer (saprolite) and the fractured bedrock, the efficiency of MAR is poorly known. To address this question and better understand the factors that control recharge dynamics, an artificial recharge basin was implemented at the Experimental Hydrogeological Park in Telangana (South India), a well-equipped and continuously monitored site situated in Archean granitic terrain. The thickness of the saprolite and hydraulic properties are relatively well known all over the site from previous geophysical surveys and hydraulic tests.

To characterize recharge dynamics, recharge has been monitored in different boreholes surrounding the infiltration basin. Infiltration rates and water level data are interpreted by both a volume balance approach and different analytical solutions. In addition, a simple numerical model was used to show how the depth of the permeable interface between saprolite and granite controls recharge dynamics and observed water levels variations. Results show that the permeability of the saprolite/bedrock interface is sufficiently large to allow an

[†]Corresponding author. Email: madeleine.nicolas@univ-rennes1.fr

efficient recharge that propagates laterally throughout the aquifer through this well connected interface. However, the variable depth of this permeable pathway controls the water level response, acting as a semi-impervious boundary, leading to remarkable water level variations. Thus, our findings show how the characteristics of the most permeable pathways control recharge dynamics in weathered crystalline rocks. In addition, we show how the depth variations of the permeable interface between saprolite and granite may be inferred from the monitoring of water level during recharge events.

Highlights

- Preferential flow in the weathering interface controls recharge propagation
- Variable bedrock relief causes aquifer compartmentalization and focused recharge
- Modeling shows compartment dimensions control the rate and amplitude of WL increase

Keywords: Managed Aquifer Recharge, Crystalline rock aquifers, Compartmentalization, Bedrock topography, Weathering interface, Numerical modeling

Funding

This work has mainly benefited from CARNOT Institute BRGM funding. The Choutuppal Experimental Hydrogeological Park has also benefited from INSU support within the H+ observatory.

Declaration of interest

None

List of abbreviations

α : Coefficient of proportionality between infiltration and water level in the basin (dimensionless)

b : Original saturated thickness (L)

$\bar{b}$: Average saturated thickness (L)

E : Evaporation (L/T)

h : Water table elevation above the base of the aquifer (L)

h_{sim} : Simulated water table elevation above the base of the aquifer (L)

h_{obs} : Observed water table elevation above the base of the aquifer (L)

H : Water level in the basin (L)

Inf : Infiltration (L/T)

K : Horizontal permeability/ hydraulic conductivity (L/T)

K_V : Vertical permeability/ hydraulic conductivity (L/T)

L_b : Length of rectangular recharge basin (L)

L : Aquifer thickness (L)

P : Precipitations (L/T)

Q_{in} : Supply canal input (L/T)

R : Recharge rate (L/T)

$RMSE$: Root Mean Square Error

S : Storativity (dimensionless)

t : Time (T)

T : Transmissivity (L^2/T)

VBA : Volume Balance Approach

W_b : Width of rectangular recharge basin (L)

x, y : Cartesian coordinates with center of recharge basin as origin (L)

1. Introduction

Despite their low yields and complexity (Roques *et al.*, 2016), many regions in the world depend on fractured crystalline aquifers as the only source of freshwater (UNESCO, 1999), particularly in arid and semi-arid regions like India. Crystalline rocks cover about 70% of India's geographical area (Saha *et al.*, 2013). Furthermore, India has seen an unprecedented development of groundwater exploitation within the last 50 to 60 years. Irrigation potential increased from 6.5 M ha to 45.7 M ha (Sharma et al., 2005), out of which it is estimated crystalline rock aquifer groundwater represents more than 50%, especially in South India (Planning Commission, 2011). The advent of this "Green Revolution", aimed towards increasing agricultural output and achieving food security, has also brought on a number of water scarcity and groundwater quality degradation issues (Pingali, 2012; Pinstrup-Andersen & Hazell, 1985; R. Singh, 2000). Natural replenishment of groundwater reservoirs has become insufficient to keep pace with the excessive continued exploitation of groundwater resources in many regions, leading to a long-term drop of groundwater levels (Central Ground Water Board, 2013).

In this context, the government has set out to remediate water table depletion by increasing aquifer recharge from 9% of total rainfall under natural conditions to 15% by 2020 (Government of Andhra Pradesh, 2003) through the development of large-scale managed aquifer recharge (MAR) schemes. The Central Ground Water Board has proposed the building of 11 million MAR structures nation-wide, as well as the reparation, renovation and restoration of the already existing structures, the total costs tallying up to over 12bn USD (Central Ground Water Board, 2013). A wide spectrum of MAR techniques may be implemented to recharge the groundwater reservoir, and these are selected mainly in terms of the hydrogeological framework. For example, infiltration methods (such as percolation tanks) are prioritized in relatively permeable environments, such as alluvial formations, while recharge shafts are preferred when the aquifer is overlain by poorly permeable strata; injection wells are used if the aquifer is confined. In India, and in the state of Telangana, underlain mainly by hard rock, the most prevalent recharge structures are percolation tanks and infiltration basins (Central Ground Water Board, 2013). It was estimated in the latest census of Minor Irrigation Sources that there are 46,531 percolation tanks, all of which the Department of Irrigation has set out to restore by 2020 (Irrigation & CAD Department, 2015).

MAR can be used to address a wide range of water management issues, including: reducing seawater intrusion or land subsidence (e.g. Masciopinto, 2013), smoothing out supply and demand fluctuations (e.g. Palma et al., 2015), protecting groundwater-dependent ecosystems (e.g. Ward & Dillon, 2012), and improving water quality through filtration and chemical and biological processes (e.g. Hamadeh et al., 2014). In this particular case, however, MAR is only expected to remediate groundwater exploitation, and water quality is not managed (Jakeman et al., 2016).

Overall, common belief is that MAR initiatives are a viable and suitable solution to water scarcity issues. However, there is little consensus within published studies about their efficiency and impact, especially in hard rock context. At small scales (a few square meters to a few square kilometers), results often point towards increased groundwater resources and predominantly positive impacts of artificial recharge (Massuel *et al.*, 2014; Srivastava *et al.*, 2009), which benefit only landholders closest to the recharge facilities (Boisson et al., 2015b; Dillon et al., 2009). Larger-scale studies (at the watershed scale or bigger) are less common (e.g. Glendenning *et al.*, 2012), on one hand, because of the difficulty in obtaining relevant data (de Marsily *et al.*, 2005), and on the other on the complexity associated with groundwater reservoirs in crystalline rock. Further, many of these studies are limited to water budget analysis and do not focus on hydrodynamic processes (e.g. Scanlon *et al.*, 2012; Boisson *et al.*, 2015b). While water budgets can provide useful guidelines for groundwater exploitation, many authors have pointed out their insufficiency in providing accurate estimates of safe yield and sustainability, highlighting the need to understand dynamic processes (Bredehoeft, 2002; Zhou, 2009). Information on dynamic processes is further necessary to make out the spatial distribution of artificial recharge.

Weathered crystalline rock aquifers are characterized by highly variable hydraulic properties (Acworth, 1987; Chilton & Foster, 1995; Dewandel *et al.*, 2012; Maréchal *et al.*, 2004) which result in a complex combination of diffuse recharge and preferential flows (Alazard *et al.*, 2016; Reddy *et al.*, 2009; Sukhija *et al.*, 2003), where the latter have often been shown to dominate groundwater recharge processes (Cuthbert & Tindimugaya, 2010; Gleeson *et al.*, 2009; Sukhija *et al.*, 2003). In the aquifer, horizontal preferential flows take place in the most transmissive zones of the aquifer, which consist of the main open fractures and most importantly the bedrock weathering interface at the limit between the upper weathered layer (saprolite) and the fractured granite; this

has been recognized by many authors (e.g. Acworth, 1987; Chilton & Foster, 1995; Dewandel *et al.*, 2006; Boisson *et al.*, 2015a). The presence of these zones leads to a vertical anisotropy of permeability (Maréchal *et al.*, 2004, 2003). Since the bedrock weathering interface is in general hilly, its relief may control groundwater flows, leading to aquifer compartmentalization, where exchanges between compartments depend on water levels relative to interface topography (Guihéneuf *et al.*, 2014). The exact nature of the relationship between the bedrock weathering interface relief and recharge is not yet clearly understood. While this study focuses on fractured crystalline rock, it should be noted that the existence of sub-horizontal preferential flow pathways originating from sharp vertical contrasts in transmissivity exists in other type of media as well, such as stratified aquifers (Nimmo et al., 2017), and that the observations outlined in this paper may be applicable in these environments as well.

Artificial recharge may be affected by preferential flow paths in contrasting ways. Their existence could enhance recharge, allowing an efficient and rapid lateral transfer of percolation throughout the aquifer. On the other hand, the compartmentalization associated with these environments highlighted by previous studies, could possibly slow or stop the progression of infiltration fronts leading to focused recharge in specific areas. Monitoring of MAR infiltration front progression is therefore necessary to better understand the role of preferential flow paths on the efficiency of recharge processes in crystalline rock aquifers, not only from a quantitative standpoint but also in regards to water quality and pollution propagation issues.

The aim of this study is to characterize artificial recharge processes in weathered crystalline rock and analyze the complex flow dynamics of recharge inputs through the main flow paths, namely the relief of the saprolite/bedrock interface. To do so, we monitored an artificial recharge basin that has been set up in an experimental site equipped with a network of observation borewells. A water balance and simple infiltration equations were used to quantify the inputs of the recharge basin and their temporal evolution, as well as the vertical hydraulic properties. Then, the lateral progression of the infiltration front in the underlying hard rock reservoir was analyzed. Analytical solutions were used to infer the lateral hydrodynamic properties of the media, while numerical modeling allowed us to quantify the effects of basement relief on recharge in order to explain the particularities of the observed recharge process.

2. Study site

The infiltration basin is situated within the Experimental Hydrogeological Park (EHP), which is a hydrological observatory located near the Choutuppal village in the Nalgonda district (Telangana state since 2014), 60 km to the south-east of Hyderabad (Latitude: 17°17'47"N; Longitude: 78°55'12"E), in South India (Fig. 1). The site has been developed by the French Geological Survey (BRGM) in partnership with the Indian National Geophysical Research Institute (NGRI) and is part of the H+ Observatory network. Most data used in this study can be downloaded from the H+ database (http://hplus.ore.fr/en).

2.1 Geological setting

The site is located in an Archean granite setting, which represents over 80% of the total surface of the Telangana state. This granitic formation is intruded locally by geological discontinuities such as dikes or quartz reefs, but none are present on the EHP (Guihéneuf *et al.*, 2014). The fracturing of the granite is mainly characterized by sub-horizontal fractures, which can display a lateral extension of tens of meters (Guihéneuf *et al.*, 2014). The typical geological profile in the EHP was obtained through analysis of drilling cuttings, and generally follows the description provided in Dewandel *et al.* (2006), namely:

- A thin red soil layer (a few centimeters).
- A sandy regolith layer 0-2 m thick, made up of a sandy-clay composition with quartz grains (Dewandel *et al.*, 2006).
- A laminated saprolite layer of variable thickness (ranging from 0 to 20m), derived from in-situ weathering of granite. It presents a millimeter-spaced horizontal laminated structure and coarse sand-size clasts and a few preserved conductive fractures (Dewandel *et al.*, 2006). Due to its composition, the saprolite layer can reach a quite high porosity (bulk porosities are mainly between 5% and 30%), depending on the lithology of the parent rock and the degree of weathering (Dewandel *et al.*, 2006).
- Granite mainly consisting of quartz, potassium feldspars and biotite (Dewandel *et al.*, 2006). The few first meters of the granite, in contact with the laminated saprolite (i.e. the saprolite/granite interface), are highly weathered and fractured. The fracture density rapidly decreases with depth, although local transmissive fractures may be encountered up to 60 meters deep (Guihéneuf *et al.*, 2014) . The effective

porosity of this layer is relatively low, of about 1%, and in mainly ensured by the fissure zones (Dewandel *et al.*, 2006).

Fig. 1: Study site location and position relative to Hyderabad (a, b), the Musi River and the supply channel (c); borewell position within EHP site (d, e, f), orange points are those equipped with pressure sensors.

2.2 Hydrological setting

The climate of this region is semi-arid and controlled by the periodicity of monsoons. Mean annual temperature is 28°C with high temperatures of about 45°C during the dry season. The rainy season occurs from June to November for a yearly average of about 800 mm. Ephemeral streams may be present during the monsoon but are most of the time absent. Intra-seasonal water level variations depend on groundwater recharge but are generally comprised between 10 and 20 m below ground surface (m bgs) (Fig. 2). There is no apparent straightforward relation between rainfall episodes and water level variations, and some intense rainfall episodes do not elicit a groundwater response (like in 2012, 765 mm of rain, Fig. 2).

Fig. 2: Hydraulic head variations in the CH03 borewell (longest on-site observed time series) and rainfall. Recharge basin was first filled by the end of 2015 (black arrow). The horizontal gray line illustrates the limit between the saprolite and the granite determined from borehole cuttings. For information relating to technical specificities of the well, refer to Guihéneuf (2014)

Within the framework of the previously cited state-wise MAR project, an infiltration basin was dug on the EHP during 2015 to meet the demands of farmers in the area facing water scarcity. Land use in the vicinity of the observatory consists mostly of cotton fields, some rice paddies and a few orchards, although it is assumed pumping for irrigation does not impact water levels on the site as most pumped borewells are downstream from the site. The basin was dug using an excavator; its approximate dimensions are 120 m by 40 m, with a depth of about 2 m, effectively removing the regolith layer and extending into the saprolite. Debris was piled around the basin to create a bund and avoid spillovers. The basin is mainly supplied by a canal which deviates water from the Musi River, downstream the state capital, Hyderabad (Fig. 1). The distance traveled by the canal between the Musi River and our study site is of about 40 km. Over this distance, the canal branches out into several smaller canals, which supply a network of infiltration basins throughout the region. The water thus used to recharge aquifers is river water directly rerouted into the subsurface without any treatment whatsoever. Unfortunately, despite several attempts by various governments, the river Musi is the eighth

most polluted river in India, receiving nearly 645 million liters per day of sewage water (Nilesh, 2016), as well as industrial effluents let out by pharmaceutical and bulk drug companies (Cheepi, 2012; Nitin, 2018).

The basin was initially filled by the end of 2015 (black arrow, Fig. 2), but this period was not yet monitored. The continuous monitoring of the basin began during the following filling episode which took place in July 2016. Groundwater levels significantly increased following the filling of the basin, reaching the highest levels ever monitored on-site (Fig. 2). Note that in many countries, regulations state the need for an infiltration basin and the underlying aquifer to remain hydraulically disconnected (Bouwer, 2002; Carleton, 2010; Réfloch, 2018). This allows preservation of an unsaturated zone below the basin, which is necessary to allow aerobic processes to take place to partly prevent the propagation of contaminants. This criterion was not met during this study because the water supply relied on the sporadic opening of an upstream floodgate managed by a third party entity.

Fig. 3: Conceptual model of transmissivity (T) and storativity (S) profiles by depth extrapolated from several hydraulic tests performed on-site by from Boisson *et al.* (2015) and schematic representation of geological log (adapted from Boisson *et al.*, 2015a). Storativity measurements end at the top of the fissured bedrock because they could not be measured within the saprolite at the time of the study as the boreholes are fully cased down to the contact between saprolite and fissured bedrock

Previous works (e.g. Guihéneuf *et al.*, 2014; Boisson *et al.*, 2015a), during which a series of hydraulic tests were performed on-site, have allowed the estimation of the media's hydrodynamic properties (Fig. 3), namely the transmissivity (T, $m^2.s^{-1}$) and storativity (S). The upper fractured granite and the fractures within the granite were shown to be the most conductive with a good storativity (Fig. 3, Boisson *et al.*, 2015a). On the other hand, the saprolite layer was characterized as poorly transmissive. It must be noted, however, that several authors have suggested the potential of preserved fractures within the weathered saprolite to contribute to preferential flow (Dewandel et al., 2006; Perrin et al., 2011), and that overall knowledge on saprolite properties is currently limited.

In sum, the most transmissive zones of the aquifer are the upper fractured zone also known as the weathering interface, laterally well connected, and some permeable fractures encountered at greater depths, which conversely have a limited extension and continuity. Because the weathering interface has a variable depth (Dewandel *et al.*, 2006; St. Clair *et al.*, 2015), groundwater flow dynamics shift depending on water table

elevation (Guihéneuf *et al.*, 2014). In the 2014 paper by Guihéneuf *et al.*, hydraulic tests performed under different water level conditions (high water levels and low water levels), in combination with observations on piezometric variations, revealed how aquifer compartmentalization causes this contrasting behavior. Under high-level conditions, the well-connected permeable upper granite/saprolite zone allows regional flows to take place, more specifically towards the northeast of the site (Guihéneuf *et al.*, 2014). Contrariwise, because fracture density and therefore connectivity decreases with depth, low water levels lead to a lateral compartmentalization of the aquifer. The system then shifts to an independent local flow system (Guihéneuf *et al.*, 2014).

The site is equipped with 30 borewells of different depths (Fig. 1), all of which are equipped with a casing extending into the saprolite, screened or open at the contact zone between the saprolite and the fractured granite. Tab. 1 features the technical characteristics of the site boreholes which were used for this study, and the hydraulic properties at each of these wells may be found in Guihéneuf et al. (2014). Note that the saprolite thickness, which ranges from 14 m to 24 m, is very variable (Tab. 1). 8 boreholes were continuously equipped with pressure and temperature sensors measuring piezometric levels and temperature during the time of this study. An additional probe was installed in the infiltration basin to monitor water levels in the basin. At the time-scales considered, the fracture system within the fractured granite and the overlying saprolite are assumed to be at equilibrium, meaning there is no significant pressure difference between the unconsolidated saprolite and the fractures in the underlying granite. This was later confirmed when superficial wells (<15 m) were dug only in the saprolite near the CH01 and CH02 boreholes (Fig. 1f) which featured virtually the same hydraulic head variations as the deeper wells. This is consistent with the unconfined response (high storativity, Fig. 3) of the interface to pumping tests under packers which confirms the role of vertical fractures in connecting overlying saprolite with underlying fractures.

	X (m)	Y (m)	Elevation (m asl)	Borehole depth (m)	Casing depth (m bgs)	Estimated saprolite thickness (m)
CH01	279075.05	1913316.12	365.69	73.20	23.90	24.00
CH02	279120.68	1913296.32	366.31	73.20	18.75	19.00
CH03	278906.31	1913534.27	365.63	50.30	14.20	14.70
CH08	278876.59	1913531.05	366.11	61.00	17.30	18.00
CH11	278904.75	1913564.44	365.70	56.40	21.00	19.50
CH15	278949.36	1913522.31	364.60	56.40	18.30	17.90
CH16	278956.63	1913558.42	364.61	56.40	17.30	15.20
CH18	278914.12	1913576.32	365.57	50.30	19.80	21.35

Tab. 1: Boreholes characteristics of the Experimental Hydrogeological Park in Choutuppal (Andhra Pradesh, Southern India) from Guihéneuf et al. (2014). Boreholes location is provided in the UTM projected coordinate system. Borehole depth and casing depth are given in meters below ground surface.

2.3 Water level variations in response to recharge

The filling of the artificial recharge basin caused water levels to rise significantly (Fig. 4). The basin remained flooded for most of the observation period, although levels in the basin varied widely from a few cm up to almost 3 m depending on the sporadic canal inputs. Each filling episode was followed by a recession period ranging from a few days to a few months, becoming longer towards the end of the observation period.

Borewells can be divided into two groups relative to their groundwater level variations. The first, composed of CH01 and CH02, is the cluster closest to the basin. The second comprises the boreholes in the cluster farthest from the basin (CH03 to CH24), out of which only 3 are shown along the AB profile (Fig. 4) for clarity purposes. The two groups are characterized by different patterns of water level variations but have similarities between them. There are three identifiable phases for both clusters depending on the time, *t*, of observation, starting from t=0, which is the beginning of the monitoring period (July 5th 2016):

- **P1** $0 < t < 60$ days (approx.). The overall range of variations is weak. The water levels for neighboring boreholes (CH01 and CH02) remain deep (about 15 m below surface) close to water levels observed before basin infilling. This suggests the water table remains disconnected from the infiltration basin during this period of time.

- **P2** $60 < t < 80$ days (approx.). An abrupt increase in water levels, of about 15 m, is observed for neighboring boreholes (CH01 and CH02), while the basin water levels vary between 1 and 2 meters. During this period, hydraulic head reaches near-surface levels (CH02 is at 366.3 m asl and CH01 at 365.7 m asl). Such variations suggest that the basin and the aquifer are becoming hydraulically connected. The increase in remote water levels (CH03 to CH24) is much weaker but shows a clear response. This phase ends at around 80 days, where an important inflection point can be observed (Fig. 4) marking a change in dynamics.
- **P3** $t > 80$ days. For this period of time, water levels in the closest boreholes (CH01 and CH02) are very high, close to ground surface levels suggesting that the basin remains connected to the water table. Remote boreholes appear to increase strongly during the first 40 days where water levels reach a depth of only a few meters below ground. Interestingly, remote borehole levels appear to evolve in sync with very similar hydraulic heads measured in all boreholes.

These observations suggest that P2 is a transition phase between the disconnected phase P1 and the fully connected phase P3 during which the basin fills the whole aquifer. Accordingly, the hydraulic response for remote boreholes is delayed in relation to neighboring boreholes. When levels in the near vicinity reach a pseudo-steady-state, remote water levels begin increasing simultaneously. This indicates a sort of tipping point mechanism: the attenuation of water level increase in the near vicinity of the basin is related to the progression of the pressure front laterally.

Fig. 4: Basin water level variations (gray curve) and associated hydraulic head variations in site boreholes shown in Fig. 1. Only 3 boreholes are shown for clarity purposes, as variations between neighboring boreholes was very similar.

3. Methods

The methodology applied aims to characterize the hydraulic properties controlling infiltration and its lateral transmission throughout the aquifer, as well as the effects of bedrock topography on the transient aquifer response. This was done through a combination of analytical and numerical modeling using water levels in the basin, meteorological data (rainfall and potential evapotranspiration) and the observed water level response in the observation boreholes. Daily rainfall was measured on-site using an automatic weather station, and daily

open pan evaporation was measured and made available by ICRISAT (International Crops Research Institute for the Semi-Arid Tropics, about 80 km away from our site).

3.1 Estimating infiltration rates and vertical hydraulic conductivity

Infiltration (Inf) from the basin into the aquifer was quantified to characterize recharge, and to be used as inputs to the analytical and numerical aquifer response models posteriorly described. To do so, a volume balance approach (VBA) was applied in parallel to infiltration equations that will be described hereafter.

The VBA approach requires knowledge of all of the water balance components: canal inflow Q_{in}, rainfall P, evaporation E, and basin stock variations dH, all of which are in mm/day:

$$Inf = Q_{in} + P - E - dH \quad (1)$$

It was assumed that the runoff component, considering the small impluvium surface (<1ha), was negligible. Because it was not possible to measure canal inflow directly for technical reasons, the VBA approach was only applied to recession periods, where Q_{in} is assumed to be null. dH was deduced from the water levels measured continuously in the basin (H) where $dH = H_t - H_{t-1}$. E was assumed to be equal to open pan potential evaporation measurements. The equation was applied at a daily time step. The VBA approach is the most complete as it accounts for all inputs and outputs to the system although it is not applicable during basin filling periods.

In the absence of rainfall and neglecting evaporation, one also expects infiltration rates to be simply related to water levels in the basin, with greater water levels leading to greater infiltration. To examine such relationships, infiltration rates from basin water level variations during recession periods were compared to the corresponding water levels in the basin. Thus, the relationship $Inf = \alpha \times H$ (with α as the coefficient of proportionality) was evaluated empirically. If a satisfactory relationship is obtained during recession periods, such relationship may be extrapolated to all times, including infilling periods. Comparison to VBA infiltration ensured that neglecting P and E is not too strong of an assumption. Finally, with infiltration roughly deduced from basin water levels, the canal inflow Q_{in} can be calculated during infilling periods as the remnant of Eq. 1.

Note that these relationships can generally be described by Darcy-type equations, directly linking infiltration to water levels based on knowledge of saturated thickness and hydraulic conductivity (Bouwer, 2002). It was not possible to estimate hydraulic conductivity during the initial phases (P1 and P2) because the depth of the wetting front and the apparent hydraulic conductivity are poorly constrained in partially saturated environments.

When there is a full hydraulic connection between the basin and the aquifer (P3), one may assume that the system may be equated to a falling head permeameter during the recession periods. Flows are assumed to be mainly vertical within the saprolite before reaching the weathering interface, which is assumed to be an a priori much more conductive zone. It therefore is assumed that flows are mainly controlled by the saprolite's properties, which offer the greater resistance to flow, and the head gradient over the saprolite's thickness. The hydraulic head at the bottom of the saprolite may be given by the hydraulic head in the closest boreholes, which are very close to ground level. Thus, the head gradient may be roughly estimated equal to H/L, i.e. the difference in hydraulic head between the top of the saprolite ($H + L$) and the bottom of the saprolite (L), with L the thickness of the saprolite. The vertical flow can be thus described using the Darcy equation:

$$Inf = K_V \frac{H}{L} \quad (2)$$

where K_V is the vertical hydraulic conductivity (L.T^{-1}). Knowing that $Inf \approx -\frac{dH}{dt}$ during recession periods, this equation can be rearranged to yield $-\frac{dH}{H} = \frac{K_V}{L} dt$, where the boundary conditions of this problem are $H = H_0$ at $t = 0$. If we integrate dH/H on the left hand side from H_0 to H and the right hand side from 0 to t, then $ln\left(\frac{H_0}{H}\right) = \frac{K_V}{L} t$. This yields:

$$\frac{H}{H_0} = e^{\frac{-K_V}{L} t} \quad (3)$$

To check the consistency of the above equation, observed water levels were plotted for each recession posterior to hydraulic connection (P3 phase). When verified, a linear regression allows estimating of $-\frac{K_V}{L}$, and with known L hydraulic conductivity can be deduced. Finally, having estimated K_V during recession period allows estimating infiltration also for the infilling periods using Eq. 2.

3.2 Modeling the aquifer response to infiltration

In a second step, we calibrated an analytical solution modeling groundwater level variations against observations to provide an estimate of the hydrodynamic parameters controlling lateral flow. The effects of the transmissive interface's relief on flow, however, were ascertained using simple numerical modeling since no analytical solution was available for this purpose. To do so, different scenarios were tested where bedrock relief and hydrodynamic properties were varied to assess the changes in groundwater response, and the overall likeness to the dynamics observed on the experimental site.

3.2.1 Analytical solutions

Calibration of simple analytical solutions against observed groundwater levels can allow a first-order estimation of the horizontal hydraulic conductivity and storativity controlling groundwater flow.

Groundwater mechanisms are described by different mathematical models depending whether there is a hydraulic connection between the basin and the water table or not (Fig. 5). The most common analytical solutions for groundwater mounding are valid only in situations where the water table is assumed to be hydraulically disconnected from the bottom of the groundwater infiltration basin. Conversely, analytical modeling of mounds that are fully connected to any recharge structure is relatively rare and most often concerns streams or canals (e.g. Dillon & Liggett, 1983; Spanoudaki *et al.*, 2010); modeling of connected recharge basins or lagoons (e.g. Kacimov *et al.*, 2016) is much rarer. Further, if the mechanisms in place deviate from standard conditions assuming homogeneous media, then fully realistic descriptions of these processes are said to be beyond any simple analytical solutions (Alderwish, 2010). In this context, it was decided to use analytical modeling only in the initial phase of wetting and mounding (P1), when the recharge basin is clearly disconnected from the aquifer and thus flow conditions remain relatively simple and respect the initial conditions required. Because remote boreholes (CH03 to CH24) show little to no response during this phase, analytical modeling was only calibrated against observations in neighboring boreholes (CH01 and CH02), which show a clear response to basin infilling even during the initial phase of wetting and mounding (P1). We used Hantush's solution for rectangular basins (Hantush, 1967).

3.2.1.1 Hantush's solution for rectangular basins

In general, analytical solutions to predict the rate of growth and shape of a recharge mound solve the governing partial differential equation describing the flow of groundwater as given by the linearized Boussinesq equation (Warner *et al.*, 1989):

$$K\bar{b}\left(\frac{\partial^2 h}{\partial x^2}+\frac{\partial^2 h}{\partial y^2}\right)+R=S\frac{\partial h}{\partial t} \quad (4)$$

where the different variables and parameters are defined in Fig. 5. The solution developed by Hantush (Hantush, 1967) simulates groundwater mound growth and decay in response to percolation, and is valid when the top of the groundwater mound is disconnected from the bottom of the recharge basin:

$$Z=\frac{R\bar{b}}{2S}\int_0^t\left(\mathrm{erf}\left(\frac{\frac{L_b}{2}+x}{\sqrt{4\upsilon\tau}}\right)+\mathrm{erf}\left(\frac{\frac{L_b}{2}-x}{\sqrt{4\upsilon\tau}}\right)\right)*\left(\mathrm{erf}\left(\frac{\frac{W_b}{2}+y}{\sqrt{4\upsilon\tau}}\right)+\mathrm{erf}\left(\frac{\frac{W_b}{2}-y}{\sqrt{4\upsilon\tau}}\right)\right)d\tau \quad (5)$$

where $Z=h^2-b^2$, υ is a simplifying term with $\upsilon=K\bar{b}/S$ and $\tau=(t-t')$, the time during which percolation takes place. Initial conditions assume a horizontal water table and the boundary conditions of zero slope of the mound profile at the center of the basin and at infinity.

Fig. 5 : Schematic representation of water level variations in response to artificial recharge from an infiltration basin featuring parameters used in analytical modeling of artificial recharge (adapted from Warner *et al.*, 1989)

In Eq. 5, recharge from infiltration is assumed to be constant. However, infiltration was found to vary significantly in time. To get around this issue the approach was modified: rather than directly integrating Eq. 5 by Gauss quadrature, a convolution of the impulse response of the aquifer to $R=1$ and the daily infiltration time-series was made, so that at a given time t:

$$Z(t)=\sum_{k=1}^{t}Z_{k-1}+ZU(k)*R(t-k) \quad (6)$$

where ZU is the impulse response and R is the recharge rate assumed equal to daily infiltration. This solution was applied and calibrated at each borehole for which hydraulic head measurements are available, where x, y, b, and $\bar{b}$ were set to match the borehole's position and initial water table conditions.

Hydraulic conductivity (K) and storativity (S) were obtained by optimizing the analytical models' performance, i.e. minimizing the root mean square error (RMSE) between h_{sim} (simulated water table elevation) and h_{obs} (observed water table elevation). The 2D parameter space was thus explored in order to reach a parameter set for which the error was minimal and which fit realistic standards. The resulting 2D RMSE matrix was then analyzed to assess whether the model converged towards a unique solution, as opposed to a situation where there is equifinality of parameters, which implies there are several acceptable sets of parameters that cannot easily be dismissed and should be considered in the evaluation of uncertainty (Beven, 2006).

Because this solution simulates how recharge inputs move laterally throughout the aquifer, and considering the important vertical anisotropy of hydraulic conductivity in fractured crystalline aquifers (Maréchal *et al.*, 2004, 2003), K is assimilated to horizontal hydraulic conductivity.

3.2.2 Numerical modeling for connected basin

While analytical solutions are easily and straightforwardly applied, they do not account for the geometry of the aquifer and specific boundary conditions. Under these circumstances, we tested the effect of bedrock relief on drawup, i.e. the increase of water level due to basin infiltration, using MODFLOW and its BCF2 package (which allows wetting of previously dry cells) (Harbaugh, 2005). MODFLOW is a US Geological Survey block-centered finite-difference modular flow model, and the source code is free public domain software. The model was run using FloPy (Bakker *et al.*, 2016), a Python package for creating, running and post-processing MODFLOW-based models.

The numerical simulations were based on very simple conceptual models. First, a synthetic scenario with constant recharge was tested in order to analyze the causal relationship between the boundary conditions imposed by the bedrock relief and the groundwater response to recharge. Synthetic results were roughly compared to field results. At this stage however the objective was not to attempt to perfectly match the observed groundwater response to infiltration. Then, in a second step aimed at better reproducing the recharge dynamics, actual estimated infiltration rates were used as inputs to the model.

The conceptual models tested all consist of a rectangular, unconfined aquifer overlain by a thick unsaturated zone with an infiltration basin in its central part (Fig. 6). The infiltration basin covers 6400 m² and recharges the

aquifer at a rate R of 1 ×10^{-6} m.s^{-1} (about 85 mm.day^{-1}) for the synthetic tests, or at a transient rate determined by previously calculated infiltration for the final applied scenario. Recharge is applied to the highest active cell (which is automatically determined), meaning there is no retardation or storage of water in the unsaturated zone. This is equivalent to simulating a partially or fully hydraulically connected environment, i.e. P2 and P3. The initial phase P1 was not simulated due to poorly constrained boundary conditions during this unsaturated phase, and because the MODLFOW model does not accurately accommodate transient unsaturated flow. Hydraulic parameters S and K were varied over one and an half and two orders of magnitude respectively ($1 \times 10^{-3} < S < 5 \times 10^{-2}$ and $1 \times 10^{-5} < K < 1 \times 10^{-3}$ m.s^{-1}) to test the sensitivity of the model to these parameters while remaining in a realistic range and were later fixed respectively at 1×10^{-2} and 1×10^{-4} m.s^{-1} to match the first-order estimation of parameters from the analytical model for the synthetic tests, or more precise values for the applied scenario. The ratio of vertical to horizontal conductivity was fixed at 1/10 according to Maréchal *et al.* (2004) results.

We only simulate one quadrant of the aquifer (Fig. 6a) because all four quadrants are symmetrical (therefore there is no flow between quadrants). The hydrological system was simulated using a grid of 100 rows and columns with a 20 m spacing (for a total model size of 2000×2000 m, size at which it was estimated the outer boundary conditions did not affect the results for the simulated duration) and six 5 m thick layers (necessary to model stability) (Fig. 6b). To ensure that the grid size and disposition were stable tests were performed where the size of the model and of the grid cells were varied to ensure water levels near the boundary remained stable. Initially, layers 1-5 are dry, head is 5 m and only the deepest layer is saturated. The evolution of the groundwater mound over time was modeled using a transient simulation, which was run for one stress period of 300 days with a one day time step using the PCG2 solver.

Fig. 6 : Model grid (a) and layer (b) configuration used for numerical modeling (adapted from Chiang & Kinzelbach, 1992) with a conceptual 3D representation of the model's two scenarios (c)

Two scenarios were tested using two model configurations: a reference scenario, in which there is no compartmentalization, and a compartmentalized scenario where an impervious boundary was added (Fig. 6c). The reference scenario was used to simulate water table mounding resulting from local recharge in homogeneous conditions with a sub-horizontal bedrock. The other scenario accounted for the more complex

boundary conditions imposed by the basement relief, by featuring a cuboid depression at the center. The depression was aimed at representing a topographic depression at the granite/saprolite interface, as it was determined from previous Electrical Resistivity Tomography (ERT) soundings that the recharge basin is located above a bedrock depression. This was done by adding an impermeable (K and S = 1 ×10^{-20}) layer covering the bottom of the aquifer except at the center where the compartment is located (Fig. 6). We tested different compartment widths (ranging from 100 m to 1000 m with a 100 m interval) and heights (from 5 m to 25 m with a 5 m interval) to test their causal relationship to groundwater drawup dynamics.

Finally, a simulation was run using the site's actual infiltration estimations from 3.1 as inputs to account for the observed variability of inputs over time and fit the model to observations. Hydraulic parameters were set equal to those obtained with the analytical solution, only the compartment size was adjusted to fit the simulation to the observed data. This allowed us to test the model's ability to simulate the observed groundwater variations by assuming a heterogeneous basement elevation.

4. Results

4.1 Infiltration estimation and relative contributions

Estimating infiltration from the VBA (Eq. 1) or from water levels in the basin (Eq. 2) was almost equivalent. Rainfall and evaporation do not have a strong effect on stock variations, relative to canal inflow and infiltration. In total, it was estimated canal inflow accounted for 97% of inputs to the basin, and infiltration for 95% of outputs (Tab. 2): they are the main drivers of stock variations. Note that infiltration from recession periods was obtained using a volume balance approach, and then linked to water levels in the basin to obtain relationships that could be extrapolated to filling periods. These relationships were indeed found to be linear and are shown in full below. As explained in the previous section, canal inputs were estimated as the remnants of Eq. 1 with known infiltration.

Fig. 7 : Infiltration and canal inflow estimated for the observation period. Inflow is episodic and short-lived as it is controlled by the opening and closing of an upstream floodgate managed by a third-party entity.

448 Inputs from the canal are quite high (Fig. 7), and concentrated into short periods of time. Infiltration takes
449 place more homogeneously throughout the observation period, but there are still non-negligible variations that
450 mimic but do not follow perfectly water level variations (Fig. 7). Interestingly, when the recharge mound
451 reaches the base of the aquifer, between 55 and 65 days approximately, infiltration reaches its maximum value
452 around 350 mm/day for a water level in the basin close to 2.6 meters. Regardless of the large amounts of water
453 brought on afterward, and similar basin water levels, recharge remains bounded, reaching at most about 150
454 mm/day suggesting a decrease in the recharge potential. Another way to show this evolution is to investigate
455 the evolution of the relationship between daily infiltration and water levels in the basin (Fig. 8a) for each

Fig. 8 : Infiltration relative to water levels in the basin for each phase of infiltration (a) and proportionality coefficients between infiltration and basin water levels plotted as a function of time. Proportionality coefficients are obtained for each individual recession period following the equation $Inf = \alpha \times H$ (b).

456 recession period.

457 Infiltration is roughly proportional to water levels in the basin, as expected from Eq. 2, but with different
458 relations for the different period of recessions. The coefficient of proportionality, α, decreases strongly with
459 time (Fig. 8b) during phase P2. For times greater than 80 days (P3), no significant changes are observed,
460 however the efficiency of the infiltration seems to be reduced by a factor of 6 from the early times until 80
461 days. This behavior is expected when connecting the basin with the aquifer (Bouwer, 2002; Carleton, 2010)
462 because of the decrease in hydraulic gradient which results from the pore space filling up at the point of
463 hydraulic connection. This further supports the statement that P2 is a transition phase during which the basin
464 becomes hydraulically connected to the aquifer.

465

	Total contribution (mm)	Relative contribution (%)
Rainfall	680	3
Canal inflow	19,230	97
Total estimated input	19,900	100
Pan evaporation	960	5
Infiltration	19,140	95
Total estimated output	20,100	100

466 Tab. 2: Contributions of water budget components

4.2 Vertical hydraulic conductivity

Vertical hydraulic conductivity posterior to hydraulic connection was obtained using Eq. 3, from the recession slopes shown in Fig. 9. It was found to vary slightly between each recession slope, ranging from 7.4×10^{-6} m.s^{-1} to 9.4×10^{-6} m.s^{-1}, averaging 8.1×10^{-6} m.s^{-1}. Such values are slightly higher than what is typically expected in the saprolite in this area, but much lower than the most transmissive pathways at the interface between saprolite and the upper fractured granite (Fig. 3, Guihéneuf *et al.*, 2014; Boisson, *et al.*, 2015a).

Fig. 9 : Recession slopes when the basin is fully connected to the aquifer (P3) at an hourly time-step plotted on a semi-log axis where the slope is equal to $-\frac{K_V}{L}$ (a), and close-up of the shorter recession slopes (b). Each line corresponds to a different recession slope; five different recessions are shown.

4.3 Horizontal hydraulic conductivity and storativity

Calibration of observed groundwater levels to simulated water levels for the disconnected phase (P1) using the Hantush solution resulted in the parameters summed up in Tab. 3. The best model fits can be seen in Fig. 10.

	Distance to center of basin (m)	Hydraulic conductivity K (m.s^{-1})	Storativity S (dimensionless)	$NRMSE$ (%)
CH01	100	7.0×10^{-5}	3.0×10^{-2}	1.5
CH02	67	6.0×10^{-5}	7.0×10^{-2}	1.4
	Geometric mean	6.5×10^{-5}	5.0×10^{-2}	

Tab. 3 : Hydraulic properties obtained from calibration of analytical simulations to observed hydraulic head

Fig. 10: Observed hydraulic head and simulated hydraulic head using analytical modeling in response to infiltration from the recharge basin when it is disconnected from the water table (P1) for the boreholes closest to the basin (CH01 and CH02)

RMSE was normalized by the range of variation ($NRMSE = \frac{RMSE}{h_{max} - h_{\min}}$). Model error was satisfactory, $NRMSE$s being weaker than 5%. Averaged to all boreholes hydraulic conductivity was found to be 6.5×10^{-5} m.s^{-1} with little variability between both estimates. This estimate is clearly higher than the estimate of the hydraulic conductivity of the saprolite obtained from water level recessions, averaging 8.10^{-6} m.s^{-1}, but very close to what Boisson *et al.* (2015a) and Guihéneuf *et al.* (2014) obtained for the weathering interface (Fig. 3, $\overline{T} = 1.3 \times 10^{-4}$ m^2.s^{-1} and thus $\overline{K} \approx 10^{-5}$ m.s^{-1} the interface being a few meters thick). Storativity was found to be around 5×10^{-2}, which is higher than the Fig. 3 weathering interface estimate ($\overline{S} = 9.7 \times 10^{-3}$), denoting a possible

484 influence of the saprolite on the apparent estimated storativity. According to the variations of storativity
485 between CH01 and CH02, it nevertheless seems to weaken as we move away from the basin.

486 4.4 Effect of bedrock relief (numerical model)

487 4.4.1 Synthetic scenarios

488 Synthetic results obtained from numerical simulations are shown in Fig. 11. The reference model, with
489 parameters in the range of those obtained from analytical simulations ($K = 10^{-4}$ m.s^{-1} and $S = 10^{-2}$), showed
490 very weak variations and a weak drawup slope (black curve on Fig. 11a and b), which cannot explain observed
491 water level variations from the study site. Recharge dynamics cannot be modeled satisfactorily using these
492 reasonable hydraulic parameters. Sensitivity tests (not shown in Fig. 11) were also performed on K and S. S
493 variations of one order of magnitude led to a difference lower than 2 m. Decreasing K elicited a stronger
494 groundwater response but with a weak drawup slope, again disagreeing with observed data.

Fig. 11: Simulated hydraulic head for the reference and compartmentalized scenario under constant recharge ($\boldsymbol{R}$ = 10^{-6} m.s^{-1}), where the lateral extension of the compartment is varied (a) and where the vertical extension is varied (b). Set distance to basin is 100 m. $\boldsymbol{K}$ = 10^{-4} m.s^{-1} and $\boldsymbol{S}$ = 10^{-2}

495 The most realistic simulation is obtained when considering a heterogeneous basement, and thus semi-
496 penetrating impermeable boundary conditions. The lateral extension of the depression/compartment at the
497 center of the model controls the slope of the drawup. Smaller lateral extensions of the compartment lead to
498 stronger slopes (Fig. 11a), and as the lateral compartment size is progressively increased, drawup dynamics
499 approach that of the reference scenario (i.e. no boundary effect). The vertical extension of the depression does
500 not have an impact of the slope of the drawup. It does however control the amplitude of variations (Fig. 11b),
501 where a greater difference in altitudes leads to a greater drawup amplitude.

502 4.4.2 Application to the present field case

503 The application of the compartmentalized scenario to estimated infiltration inputs proved quite successful in
504 recreating the dynamics of the closest boreholes for phase 2 and 3 (Fig. 12) using the hydraulic parameters
505 obtained from analytical modeling (Tab. 3) and varying only the shape of the basement. We obtained a

Fig. 12: Observed hydraulic head and simulated hydraulic head using numerical modeling accounting for compartmentalization in response to infiltration from the recharge basin (gray lines) for the boreholes closes to the basin (CH01 and CH02)

506 relatively good agreement between the simulated water levels and the observed ones ($NRMSE = 8.7\%$ and
507 12.1% for CH01 and CH02 respectively). The strong slope of the drawup is successfully reproduced, and the
508 following stabilization of water levels as well. A lateral extension of about 120 m seems to best recreate the
509 recharge dynamics of the study site with the above cited parameters, although storativity was shown to be
510 somewhat overestimated under the influence of the saprolite values owing to the borehole's proximity to the
511 basin. Decreasing storativity to a value closer to that of the weathering interface ($S = 9.7 \times 10^{-3}$) requires
512 increasing the theoretical lateral extension of the compartment to about 200 m to correctly model
513 observations. The calibrated vertical extension was found relatively constant, around 18 m.

514 There is a slight discrepancy between the model and the simulation, where the simulation under-estimates
515 water levels during the drawup phase and over-estimates them during P3. This is probably because the actual
516 system modeled is in reality much more complex than the model proposed here, as we do not account for flow
517 in fractures, storage effects or matrix effects. The underlying geometry of the interface may also be much more
518 complex than the way it is simulated in the model. We believe this is a testament to the interest this model
519 brings, wherein a very simple numerical model recreated complex dynamics. Note also that it was not possible
520 to simulate remote boreholes using the model as is. Placing the observation point outside of the compartment
521 did recreate the delay in borehole response observed in Fig. 4, but did not allow to simulate the amplitude of
522 the variations correctly. Addressing this issue would imply complexifying the model to account for a much
523 more complex geometry of the weathering interface, which is currently beyond the scope of this paper.

Fig. 13: Schematic representation of hydraulic head variations above the bedrock (gray area) in response to artificial recharge from a recharge basin per phase of infiltration

524 A schematic summary of recharge dynamics is presented in Fig. 13 in a very simplified way. The hydraulically
525 disconnected phase of groundwater mounding (P1) resembles that of a relatively homogeneous environment.
526 When hydraulic connection begins between the infiltration basin and the aquifer, we observe boundary
527 conditions leading to a rapid increase of water levels because infiltration is focused into a bounded domain.
528 The hydraulic connection also slows the infiltration process. The final stage P3 is much less subject to boundary
529 effects and a pseudo-steady-state is reached, where levels oscillate around a constant value.

530 # 5. Discussion

5.1 Representativity of hydraulic parameters

Overall infiltration efficiency, i.e. the ratio of infiltration to total inputs, is quite high (96%) in the present case, as opposed to previous studies in similar environments (Boisson *et al.*, 2015b: 56% ; Perrin *et al.*, 2009: 54% ; Singh *et al.*, 2004: 67%), but in agreement with efficiencies recorded by the Central Groundwater Board in 2011 of up to 98% in hard rock environments. A possible explanation of this difference is the age of the infiltration basins. Studies showing low infiltration efficiencies focused on percolation tanks that had not been recently desilted, contrary to the basin studied here (dug in 2015) and those present in the CGWB's case studies. Further, the way in which the basin is supplied, where large amounts of water are brought in short periods of time, leads to an important water depth in the basin (up to almost 3 m). This could contribute to stronger infiltration rates linked to a higher hydraulic head. This is as opposed to typical percolation tanks, which accumulate a few centimeters of runoff over larger extended areas and thus subject to a higher amount of direct evaporation compared to infiltration. Although overall infiltration efficiency is high, infiltration rates decrease significantly with hydraulic connection because of a decrease in hydraulic gradient. Infiltration is then more spread out in time, which allows more evaporation to take place, although the amount evaporated remains much weaker than the overall infiltrated volume. This is not likely to continue to be the case if significant silting occurs.

This study's estimate of vertical permeability ($K_V = 8.1 \times 10^{-6}$ m.s^{-1}), is slightly higher than what Boisson *et al.* (2015a) obtained at the same site for the upper saprolite layer (9×10^{-8} to 3×10^{-7} m.s^{-1}), but overall in the same range as other studies performed on saprolite (e.g. George, 1992: 7×10^{-6} m.s^{-1}; Cook *et al.*, 1996: 1×10^{-6} to 1×10^{-5} m.s^{-1}) . Boisson *et al.* (2015a) used falling-head borehole permeameter tests, which render point values, whereas the large horizontal extent of the infiltration basin could allow sampling of otherwise undetectable vertical preferential flow paths (i.e. preserved fractures in the saprolite), and thus lead to an increase in hydraulic conductivity (Dewandel et al., 2006).

Horizontal hydraulic properties were found to be in the upper range of values for fractured crystalline rock ($K = 6.5 \times 10^{-5}$ m.s^{-1} and $S = 5.0 \times 10^{-2}$), rather corresponding to the properties of the weathering interface obtained in Boisson *et al.*, 2015a. The horizontal hydraulic conductivity of the system is thus much higher than the vertical hydraulic conductivity (about 8 times higher). This is consistent with the fact that the vertical

hydraulic conductivity is controlled by the less transmissive saprolite, and the lateral hydraulic conductivity by the highly transmissive weathering interface acting as a preferential flow path. Overall, analytical modeling highlighted the strong influence of preferential flow in recharge processes.

5.2 Comparison to inferred interface relief

Previous acquisition of Electrical resistivity tomography (ERT) profiles (Chandra *et al.*, 2009) permitted the mapping of the depth of the weathering interface at the EHP site (Fig. 14). The ERT survey was carried out using a Syscal Jr. Switch with 10m electrode spacing across 9 profiles using a Wenner-Schlumberger configuration (Chandra *et al.*, 2009). Profiles were analyzed using a routine inversion method and a threshold of about 400 Ohm.m (Braun *et al.*, 2009) was set to delineate the limit between fresh and weathered rock (Chandra *et al.*, 2009). Point data was then interpolated using standard kriging techniques.

Fig. 14: Depth of the upper fissured layer from ERT surveys (a) and inferred 3D conceptual model of structure (b). Hypothetical compartment delimitation is the thin black lines. For clarity purposes only the wells shown in Fig. 4 are shown here.

The obtained interface is significantly hilly, composed of depressions and crests (the protruding areas), where crests delineate a set of sub-drainage basins (Fig. 14a). The hilliness of the interface relief suggests the system is compartmentalized, which supports the observations made in previous works highlighting the existence of compartmentalization in crystalline environments and its effects on groundwater flow and chemistry (e.g. Guihéneuf et al., 2014; Perrin et al., 2011). Two main compartments were identified: one east of the site and the other north of the site, extending beyond the site limits. The lowest point of the bedrock topography appears to be north of the profile. The compartment over which the infiltration basin is situated is trefoil-like-shaped, with a diameter of about 500 m, a low point at about 42m depth and summits at about 20 m depth (so a height difference of approximately 20 m). This is similar to the dimensions obtained while fitting the numerical simulation to observed water levels (i.e. a radius of 200 m and a height difference of 18 m).

Using the AB profile outlined in Fig. 4, we traced the relief of the bedrock interface obtained from ERT and replaced observed water levels so as to compare observed data to simulations (Fig. 15). The depth of the interface was very similar to the depth estimated from borehole logs. Neighboring boreholes (CH01 and CH02)

581 are situated in a topographic depression, whereas remote boreholes are in a crest area, where the two
582 compartments identified in (Fig. 14a) are separated, CH03 being at the highest point.

583 The same phases outlined in Fig. 13 can be transposed to observed data. Prior to the supposed date of
584 hydraulic connection, (in Fig. 15 $t = 0$ and $t = 40$) water level variations are weak and the water table is deep,
585 which corresponds to P1. Then, water levels increase rapidly under the effect of the lateral boundary condition
586 (in Fig. 15 $t = 60$ and $t = 70$), corresponding to P2. This continues until water levels exceed the topographic
587 threshold "downstream" from the basin at about 70 days after the beginning of the observation period. From
588 that point onwards compartments become connected and water levels vary weakly but on a large extent,
589 which corresponds to P3.

Fig. 15: Comparison of schematic representation of artificial recharge from an infiltration basin with actual hydraulic head measured on-site and aquifer geometry from ERT data

590 This conceptual model supports observations made by Guihéneuf *et al.* in 2014: the hydrogeological system is
591 compartmentalized, and the aquifer connectivity and associated flow regime is a function of water levels
592 relative to the well-connected bedrock interface.

593 5.3 Artificial recharge modeling

594 The model most commonly used to explain recharge dynamics was proposed by Bouwer (2002). In this model,
595 two scenarios explain an infiltration basin's dynamics. If the bottom of the basin (the clogging layer) is less
596 conductive than the underlying aquifer then infiltration is controlled by the hydraulic conductivity of the
597 clogging layer. The water within the basin is disconnected from the underlying aquifer, perched over the silting
598 layer. Otherwise, infiltration is controlled by the hydraulic properties of the underlying aquifer. In this case the
599 water table may rise until hydraulic connection takes place, and then the infiltration rate is controlled either
600 solely by gravity and vertical flows (in deep aquifers) or by the slope of the water table mound (in shallow
601 aquifers). This concept was developed assuming homogeneous sedimentary aquifers of infinite lateral
602 extension.

603 Instances of variable recharge dynamics have been documented in literature, either stemming from
604 progressive and heterogeneous silting (e.g. Racz *et al.*, 2012; Mawer *et al.*, 2016), saturation of the vadose zone

(Dillon & Liggett, 1983) or more rarely structural discontinuities (Massuel *et al.*, 2014). In most cases, the influence of heterogeneity on flow is limited to qualitative observations. Very few studies actually model processes with consideration of aquifer geometry (e.g. Ronayne *et al.*, 2008), probably because it is not easy to image the aquifer's geometry and practically impossible to obtain three-dimensional information about hydraulic properties, especially in hard rock context (de Marsily *et al.*, 2005). In this study we successfully quantified the role played by the basement relief (and its associated compartmentalization) on the hydraulic response of the aquifer to recharge, also highlighting the effects of it on recharge propagation and infiltration potentials. This study showed that the relief of the bedrock can produce an effect somehow analogous to the effect of impervious (or semi-impervious) boundaries on drawdown during pumping tests (de Marsily, 1986). In both cases, a change in drawdown slope relative to a situation where no impervious boundary is present is expected. To the best of our knowledge, there are no other instances in literature where this effect was identified during recharge, or as a result of a heterogeneous bedrock relief. Further, because the relief crests are only a semi-penetrating impervious boundary, the increase in drawup slope relative to the reference scenario was shown to provide information on the dimensions of the relief in question, where the larger the depression below the recharge basin the lesser the increase in drawup slope.

The in-depth analysis of the transient aquifer response to recharge in a heterogeneous environment can be used to improve MAR management in crystalline rock. The requirements to perform this type of analysis are (i) an approximation of the aquifer's hydraulic properties, (ii) a map of the contact zone between the saprolite and the granite, and (iii) knowledge on the (actual or desired) water volumes to be stored in the aquifer. The most challenging aspect of this methodology is obtaining a map of the subsurface, although geophysical methods are becoming increasingly accurate and accessible. One can, for example, cite the development of airborne electromagnetic methods, which allow large-scale high resolution mapping of the subsurface (Sørensen & Auken, 2004). However, if bedrock relief data is unobtainable, we also showed how monitoring groundwater levels in the vicinity of the basin can provide valuable information on bedrock topography and on the storage potentials of the aquifer. As such, not only should the infiltration basin be monitored, but also, if possible, groundwater levels around the basin. Extrapolation of our simple method could improve present-day forward models used for MAR management in such geological environments, and possibly be extended into predictive modeling. From a quantitative standpoint, consideration of the effects of boundary conditions would be useful

to regulate inputs in order to limit evaporation losses. If the bedrock topography is known, decision-makers can gain a greater awareness of the extent to which recharge will propagate throughout the aquifer, and choose whether to prioritize a strong localized reaction, which may be easier to retrieve at later times, or a weaker reaction over larger areas depending on the density and extent of the settlements affected by groundwater depletion and which stand to benefit from the augmentation of groundwater resources. Further, implications on water quality are also non-negligible. We highlighted the importance of preferential flow, which implies contaminant attenuation is not likely to take place rapidly enough to mitigate the negative effects of injecting wastewater into the aquifer. The dominance of advective processes over diffusive processes in hard rock (Guihéneuf *et al.*, 2017) will likely aggravate this issue. It is essential this be taken into consideration by decision-makers: the water currently used to feed the network of MAR structures state-wise originates directly from the Musi River downstream of Hyderabad and is highly polluted both by domestic and industrial effluents. Another element of risk that was identified in this study is that of hydraulic connection between the infiltration basin and the water table, to which fractured crystalline environments are particularly susceptible due to their low transmissivities and variable saprolite thickness. The best way to infer hydraulic connection is through groundwater level observation, but it is still possible to infer that hydraulic connection has taken place when infiltration rates decrease significantly (which may lead the basin to overflow or water levels in the basin to stagnate). Additionally to the loss of infiltration potentials, which may dampen the efficiency of this water stress remediation method and lead to important losses by ET, hydraulic connection may amplify the risk of groundwater contamination. If no unsaturated zone exists below the infiltration basin, aerobic processes and sorption of contaminants which play an important part in retaining and degrading contaminants, and that depend on residence times, may be impeded.

6. Conclusions

Our study of artificial recharge processes in a fractured crystalline environment highlighted the role the heterogeneity of the horizontal weathering interface depth plays on recharge. During the initial stages of wetting, when the recharge mound is disconnected from the bottom of the basin, infiltration is governed by the vertical properties of the relatively homogeneous and poorly conductive saprolite. The lateral transmission of infiltration inputs reaching the aquifer is ensured mainly by the weathering interface, thus foregrounding the

importance of preferential flows. Once hydraulic connection between the infiltration basin and the aquifer takes place, which is relatively rapidly due to the shallowness of the aquifer, two simultaneous phenomena are observed: infiltration potential decreases, and water levels increase strongly and rapidly. It was shown from numerical simulations that this can be interpreted as resulting from the control by the weathering interface relief, where summits act as semi-impervious boundaries, which delimit a set of hydrogeological compartments. The advancement of the infiltration front is thus impeded until the crest separating the east and north hydrogeological compartments is exceeded and the compartment is filled, which focuses infiltration inputs into smaller volumes, explaining the strong and sudden local water level increase. Once the summits are overpassed, the different hydrogeological compartments are connected, and the no-flow boundary effect becomes less critical.

It has yet to be confirmed if the simple analytical and numerical approach used here can be applied more generally in crystalline rock environments, but we believe this is a first step in better understanding the propagation of infiltration fronts in heterogeneous aquifers. This in turn could provide useful information for the aquifer properties and for the management of MAR structures in regards to placement, optimization, and water quality.

675 # Acknowledgments

676 This study has been carried out at the Indo-French Center for Groundwater Research (BRGM-NGRI). This work
677 has mainly benefited from CARNOT Institute BRGM funding. The Choutuppal Experimental Hydrogeological
678 Park has also benefited from INSU support within the H+ observatory. The authors are very grateful to Marion
679 Crenner and Mohammed Wajiduddin for their fieldwork, Joy Chaudhuri and Vidya Sagar for their geophysical
680 work, and Yata Ramesh, Yata Muthyalu, Pittala Krishna, Nilgonda Kishtaiah and Pittala Anjaiah for their
681 valuable on-site help. The authors are also grateful to ICRISAT for providing evaporation data. The authors are
682 thankful to the editor Peter K. Kitanidis, the associate editor and to the reviewers (John Nimmo and an
683 anonymous reviewer) for their constructive comments, which greatly enhanced the quality of the manuscript.

References

Acworth, R. I. (1987). The development of crystalline basement aquifers in a tropical environment. *Quarterly Journal of Engineering Geology and Hydrogeology*, *20*(4), 265–272. https://doi.org/10.1144/GSL.QJEG.1987.020.04.02

Alazard, M., Boisson, A., Maréchal, J. C., Perrin, J., Dewandel, B., Schwarz, T., … Ahmed, S. (2016). Investigation of recharge dynamics and flow paths in a fractured crystalline aquifer in semi-arid India using borehole logs: implications for managed aquifer recharge. *Hydrogeology Journal*, *24*(1), 35–57. https://doi.org/10.1007/s10040-015-1323-5

Alderwish, A. M. (2010). Induced recharge at new dam sites—Sana'a Basin, Yemen. *Arabian Journal of Geosciences*, *3*(3), 283–293. https://doi.org/10.1007/s12517-009-0075-8

Bakker, M., Post, V., Langevin, C. D., Hughes, J. D., White, J. T., Starn, J. J., & Fienen, M. N. (2016). Scripting MODFLOW Model Development Using Python and FloPy. *Groundwater*, *54*(5), 733–739. https://doi.org/10.1111/gwat.12413

Beven, K. (2006). A manifesto for the equifinality thesis. *Journal of Hydrology*, *320*(1–2), 18–36. https://doi.org/10.1016/j.jhydrol.2005.07.007

Boisson, A., Guihéneuf, N., Perrin, J., Bour, O., Dewandel, B., Dausse, A., … Maréchal, J. C. (2015). Determining the vertical evolution of hydrodynamic parameters in weathered and fractured south Indian crystalline-rock aquifers: insights from a study on an instrumented site. *Hydrogeology Journal*, *23*(4), 757–773. https://doi.org/10.1007/s10040-014-1226-x

Boisson, A., Villesseche, D., Baisset, M., Perrin, J., Viossanges, M., Kloppmann, W., … Ahmed, S. (2015). Questioning the impact and sustainability of percolation tanks as aquifer recharge structures in semi-arid crystalline context. *Environmental Earth Sciences*, *73*(12), 7711–7721. https://doi.org/10.1007/s12665-014-3229-2

Bouwer, H. (2002). Artificial recharge of groundwater: hydrogeology and engineering. *Hydrogeology Journal*, *10*(1), 121–142. https://doi.org/10.1007/s10040-001-0182-4

Braun, J.-J., Descloitres, M., Riotte, J., Fleury, S., Barbiéro, L., Boeglin, J.-L., … Dupré, B. (2009). Regolith mass balance inferred from combined mineralogical, geochemical and geophysical studies: Mule Hole gneissic watershed, South India. *Geochimica et Cosmochimica Acta*, *73*(4), 935–961. https://doi.org/10.1016/j.gca.2008.11.013

Bredehoeft, J. D. (2002). The Water Budget Myth Revisited: Why Hydrogeologists Model. *Ground Water*, *40*(4), 340–345. https://doi.org/10.1111/j.1745-6584.2002.tb02511.x

Brindha, K., Jagadeshan, G., Kalpana, L., & Elango, L. (2016). Fluoride in weathered rock aquifers of southern India: Managed Aquifer Recharge for mitigation. *Environmental Science and Pollution Research*, *23*(9), 8302–8316. https://doi.org/10.1007/s11356-016-6069-7

Carleton, G. B. (2010). *Simulation of Groundwater Mounding Beneath Hypothetical Stormwater Infiltration Basins*. *U.S. Geological Survey Scientific Investigations Report* (Vol. 2010–5102). Retrieved from https://pubs.usgs.gov/sir/2010/5102/support/sir2010-5102.pdf

Central Ground Water Board. (2011). *Select Case Studies: Rain Water Harvesting and Artificial Recharge*. Ministry of Water Resources, Govt. of India.

Central Ground Water Board. (2013). *Master plan for artificial recharge to ground water in India*. Ministry of Water Resources, Govt. of India.

Chandra, S., Nagaiah, E., Kumar, D., Ahmeduddin, M., Raju, K., Mallesh, D., … Ahmed, S. (2009). *Establishment of International Hydrogeological Park at Chautuppal , Nalgonda District , Andhra Pradesh Delineation of Aquifer Geometry using Electrical Resistivity Tomography : Phase-I. IFCGR Technical Report - Unpublished, 27 pp.*

---

†Corresponding author. Email: madeleine.nicolas@univ-rennes1.fr

729 Cheepi, D. P. (2012). Musi River Pollution Its Impact on Health and Economic Conditions of Down Stream
730 Villages-A Study. *IOSR Journal of Environmental Science, Toxicology and Food Technology*, *1*(4), 40–51.
731 https://doi.org/10.9790/2402-0144051

732 Chiang, W. H., & Kinzelbach, W. (1998). Processing Modflow. *A Simulation Program for Modelling Groundwater*
733 *Flow and Pollution. User Manual*. Retrieved from
734 http://www.pmwin.net/programs/prevpm/pm4/doc/pmwin41.pdf

735 Chilton, P. J., & Foster, S. S. D. (1995). Hydrogeological Characterisation And Water-Supply Potential Of
736 Basement Aquifers In Tropical Africa. *Hydrogeology Journal*, *3*(1), 36–49.
737 https://doi.org/10.1007/s100400050061

738 Cook, P. G., Solomon, D. K., Sanford, W. E., Busenberg, E., Plummer, L. N., & Poreda, R. J. (1996). Inferring
739 shallow groundwater flow in saprolite and fractured rock using environmental tracers. *Water Resources*
740 *Research*, *32*(6), 1501–1509. https://doi.org/10.1029/96WR00354

741 Cuthbert, M. O., & Tindimugaya, C. (2010). The importance of preferential flow in controlling groundwater
742 recharge in tropical Africa and implications for modelling the impact of climate change on groundwater
743 resources. *Journal of Water and Climate Change*, *1*(4), 234–245. https://doi.org/10.2166/wcc.2010.040

744 de Marsily, G. (1986). *Quantitative hydrogeology*. Paris School of Mines, Fontainebleau.

745 de Marsily, G., Delay, F., Gonçalvès, J., Renard, P., Teles, V., & Violette, S. (2005). Dealing with spatial
746 heterogeneity. *Hydrogeology Journal*, *13*(1), 161–183. https://doi.org/10.1007/s10040-004-0432-3

747 Dewandel, B., Lachassagne, P., & Krishnamurthy, N. S. (2006). A generalized 3-D geological and hydrogeological
748 conceptual model of granite aquifers controlled by single or multiphase weathering. *Journal of*
749 *Hydrology*, 260–284. https://doi.org/10.1016/j.jhydrol.2006.03.026

750 Dewandel, B., Maréchal, J. C., Bour, O., Ladouche, B., Ahmed, S., Chandra, S., & Pauwels, H. (2012). Upscaling
751 and regionalizing hydraulic conductivity and effective porosity at watershed scale in deeply weathered
752 crystalline aquifers. *Journal of Hydrology*, *416–417*, 83–97. https://doi.org/10.1016/j.jhydrol.2011.11.038

753 Dillon, P. J., Gale, I., Contreras, S., Pavelic, P., Evans, R., & Ward, J. (2009). Managing aquifer recharge and
754 discharge to sustain irrigation livelihoods under water scarcity and climate change. *IAHS-AISH Publication*,
755 *330*(September), 1–12. Retrieved from http://www.scopus.com/inward/record.url?eid=2-s2.0-
756 78751661981&partnerID=tZOtx3y1

757 Dillon, P. J., & Liggett, J. A. (1983). An ephemeral stream-aquifer interaction model. *Water Resources Research*,
758 *19*(3), 621–626. https://doi.org/10.1029/WR019i003p00621

759 George, R. J. (1992). Hydraulic properties of groundwater systems in the saprolite and sediments of the
760 wheatbelt, Western Australia. *Journal of Hydrology*, *130*(1–4), 251–278. https://doi.org/10.1016/0022-
761 1694(92)90113-A

762 Gleeson, T., Novakowski, K., & Kyser, K. T. (2009). Extremely rapid and localized recharge to a fractured rock
763 aquifer. *Journal of Hydrology*, *376*(3–4), 496–509. https://doi.org/10.1016/j.jhydrol.2009.07.056

764 Glendenning, C. J., van Ogtrop, F. F., Mishra, A. K., & Vervoort, R. W. (2012). Balancing watershed and local
765 scale impacts of rain water harvesting in India—A review. *Agricultural Water Management*, *107*, 1–13.
766 https://doi.org/10.1016/j.agwat.2012.01.011

767 Government of Andhra Pradesh. (2003). *Andhra Pradesh Water Vision-Methods, Position papers, and District*
768 *reports* (Vol. II). Water Conservation Mission, Government Insurance Building, Tilak road, Hyderabad,
769 Andhra Pradesh.

770 Guihéneuf, N. (2014). *Structure des écoulements et propriétés de transport des aquifères cristallins fracturés et*
771 *altérés : Application au site de Choutuppal (Inde du Sud)*. Université de Rennes 1.

772 Guihéneuf, N., Boisson, A., Bour, O., Dewandel, B., Perrin, J., Dausse, A., … Maréchal, J. C. (2014). Groundwater
773 flows in weathered crystalline rocks: Impact of piezometric variations and depth-dependent fracture
774 connectivity. *Journal of Hydrology*, *511*, 320–334. https://doi.org/10.1016/j.jhydrol.2014.01.061

775 Guihéneuf, N., Bour, O., Boisson, A., Le Borgne, T., Becker, M. W., Nigon, B., … Maréchal, J. C. (2017). Insights

about transport mechanisms and fracture flow channeling from multi-scale observations of tracer dispersion in shallow fractured crystalline rock. *Journal of Contaminant Hydrology*, *206*(May), 18–33. https://doi.org/10.1016/j.jconhyd.2017.09.003

Hamadeh, A. F., Sharma, S. K., & Amy, G. (2014). Comparative assessment of managed aquifer recharge versus constructed wetlands in managing chemical and microbial risks during wastewater reuse: a review. *Journal of Water Reuse and Desalination*, *4*(1), 1–8. https://doi.org/10.2166/wrd.2013.020

Hantush, M. S. (1967). Growth and decay of groundwater-mounds in response to uniform percolation. *Water Resources Research*, *3*(1), 227–234. https://doi.org/10.1029/WR003i001p00227

Harbaugh, A. W. (2005). MODFLOW-2005 , The U . S . Geological Survey Modular Ground-Water Model — the Ground-Water Flow Process. *U.S. Geological Survey Techniques and Methods*, 253.

Irrigation & CAD Department. (2015). Mission Kakatiya - Mission. Retrieved August 9, 2017, from http://missionkakatiya.cgg.gov.in/homemission

Jakeman, A. J., Barreteau, O., Hunt, R. J., Rinaudo, J.-D., & Ross, A. (2016). *Integrated Groundwater Management*. (A. J. Jakeman, O. Barreteau, R. J. Hunt, J.-D. Rinaudo, & A. Ross, Eds.), *Integrated Groundwater Management*. Cham: Springer International Publishing. https://doi.org/10.1007/978-3-319-23576-9

Kacimov, A. R., Zlotnik, V., Al-Maktoumi, A., & Al-Abri, R. (2016). Modeling of transient water table response to managed aquifer recharge: a lagoon in Muscat, Oman. *Environmental Earth Sciences*, *75*(4), 318. https://doi.org/10.1007/s12665-015-5137-5

Maréchal, J. C., Dewandel, B., & Subrahmanyam, K. (2004). Use of hydraulic tests at different scales to characterize fracture network properties in the weathered-fractured layer of a hard rock aquifer. *Water Resources Research*, *40*(11), 1–17. https://doi.org/10.1029/2004WR003137

Maréchal, J. C., Wyns, R., Lachassagne, P., Subrahmanyam, K., & Touchard, F. (2003). Anisotropie verticale de la perméabilité de l'horizon fissuré des aquifères de socle : concordance avec la structure géologique des profils d'altération. *Comptes Rendus Geoscience*, *335*(5), 451–460. https://doi.org/10.1016/S1631-0713(03)00082-8

Masciopinto, C. (2013). Management of aquifer recharge in Lebanon by removing seawater intrusion from coastal aquifers. *Journal of Environmental Management*, *130*, 306–312. https://doi.org/10.1016/j.jenvman.2013.08.021

Massuel, S., Perrin, J., Mascre, C., Mohamed, W., Boisson, A., & Ahmed, S. (2014). Managed aquifer recharge in South India: What to expect from small percolation tanks in hard rock? *Journal of Hydrology*, *512*, 157–167. https://doi.org/10.1016/j.jhydrol.2014.02.062

Mawer, C., Parsekian, A., Pidlisecky, A., & Knight, R. (2016). Characterizing Heterogeneity in Infiltration Rates During Managed Aquifer Recharge. *Groundwater*, *54*(6), 818–829. https://doi.org/10.1111/gwat.12423

Nilesh, V. (2016). Hyderabad: Pollutants in Musi rise, river becomes sewage. Retrieved December 6, 2017, from http://www.deccanchronicle.com/lifestyle/pets-and-environment/250716/hyderabad-pollutants-in-musi-rise-river-becomes-sewage.html

Nimmo, J. R., Creasey, K. M., Perkins, K. S., & Mirus, B. B. (2017). Preferential flow, diffuse flow, and perching in an interbedded fractured-rock unsaturated zone. *Hydrogeology Journal*, *25*(2), 421–444. https://doi.org/10.1007/s10040-016-1496-6

Nitin, B. (2018). A looming health threat in Hyd? How polluted Musi water finds its way back to the city. *The News Minute*. Retrieved from https://www.thenewsminute.com/article/looming-health-threat-hyd-how-polluted-musi-water-finds-its-way-back-city-87275

Palma, A., González, F., & Cruickshank, C. (2015). Managed Aquifer Recharge As a Key Element in Sonora River Basin Management, Mexico. *Journal of Hydrologic Engineering*, *20*(3), B4014004. https://doi.org/10.1061/(ASCE)HE.1943-5584.0001114

Perrin, J., Ahmed, S., & Hunkeler, D. (2011). The effects of geological heterogeneities and piezometric fluctuations on groundwater flow and chemistry in a hard-rock aquifer, southern India. *Hydrogeology*

Journal, *19*(6), 1189–1201. https://doi.org/10.1007/s10040-011-0745-y

Perrin, J., Mascre, C., Massuel, S., & Ahmed, S. (2009). Tank management in Andhra Pradesh, India: Percolation versus irrigation. In *IAHS-AISH Publication* (Vol. 330, pp. 28–33). Retrieved from https://www.scopus.com/inward/record.uri?eid=2-s2.0-78751652998&partnerID=40&md5=af84aa4600d3eeee9200c3c29c950020

Pingali, P. L. (2012). Green Revolution: Impacts, limits, and the path ahead. *Proceedings of the National Academy of Sciences*, *109*(31), 12302–12308. https://doi.org/10.1073/pnas.0912953109

Pinstrup-Andersen, P., & Hazell, P. (1985). The impact of the Green Revolution and prospects for the future. *Food Reviews International*. Retrieved from http://www.tandfonline.com/doi/pdf/10.1080/87559128509540765

Planning Commission (Government of India). (2011). *Mid-Term Appraisal Eleventh Five Year Plan 2007–2012*. New Delhi: Oxford University Press.

Racz, A. J., Fisher, A. T., Schmidt, C. M., Lockwood, B. S., & Huertos, M. L. (2012). Spatial and Temporal Infiltration Dynamics During Managed Aquifer Recharge. *Groundwater*, *50*(4), 562–570. https://doi.org/10.1111/j.1745-6584.2011.00875.x

Reddy, D. V., Nagabhushanam, P., Sukhija, B. S., & Reddy, A. G. S. (2009). Understanding hydrological processes in a highly stressed granitic aquifer in southern India. *Hydrological Processes*, *23*(9), 1282–1294. https://doi.org/10.1002/hyp.7236

Réfloch, A. (2018). *Compréhension expérimentale et numérique des chemins de l'eau sur le champ captant de la Métropole de Lyon*. Université Grenoble Alpes.

Ronayne, M. J., Gorelick, S. M., & Caers, J. (2008). Identifying discrete geologic structures that produce anomalous hydraulic response: An inverse modeling approach. *Water Resources Research*, *44*(8), 1–16. https://doi.org/10.1029/2007WR006635

Roques, C., Bour, O., Aquilina, L., & Dewandel, B. (2016). High-yielding aquifers in crystalline basement: insights about the role of fault zones, exemplified by Armorican Massif, France. *Hydrogeology Journal*, *24*(8), 2157–2170. https://doi.org/10.1007/s10040-016-1451-6

Saha, D., Dwivedi, S. N., Roy, G. K., & Reddy, D. V. (2013). Isotope-based investigation on the groundwater flow and recharge mechanism in a hard-rock aquifer system: the case of Ranchi urban area, India. *Hydrogeology Journal*, *21*(5), 1101–1115. https://doi.org/10.1007/s10040-013-0974-3

Scanlon, B. R., Faunt, C. C., Longuevergne, L., Reedy, R. C., Alley, W. M., McGuire, V. L., & McMahon, P. B. (2012). Groundwater depletion and sustainability of irrigation in the US High Plains and Central Valley. *Proceedings of the National Academy of Sciences*, *109*(24), 9320–9325. https://doi.org/10.1073/pnas.1200311109

Sharma, B. R., Villholth, K. G., & Sharma, K. D. (2005). Groundwater Research and Management: Integrating Science into Management Decisions. In B. R. Sharma, K. G. Villholth, & K. D. Sharma (Eds.), *Groundwater Governance in Asia Series - 1*. IWA Publishing.

Singh, J., Awasthi, M. K., & Sharma, R. K. (2004). Quantification of percolation from percolation Tank. *J. Soil Wat. Conserv. India*, *3 (3&4)*, 128–132.

Singh, R. (2000). Environmental consequences of agricultural development: a case study from the Green Revolution state of Haryana, India. *Agriculture, Ecosystems & Environment*, *82*(1–3), 97–103. https://doi.org/10.1016/S0167-8809(00)00219-X

Sørensen, K. I., & Auken, E. (2004). SkyTEM - a new high-resolution helicopter transient electromagnetic system. *Exploration Geophysics*, *35*(3), 194. https://doi.org/10.1071/EG04194

Spanoudaki, K., Paschalinos, Y., Memos, C. D., & Stamou, A. I. (2010). Analytical Solution to the Stream-Aquifer Interaction Problem: A Critical Review. *Global Nest Journal*, *12*(2), 126–139.

Srivastava, R. C., Kannan, K., Mohanty, S., Nanda, P., Sahoo, N., Mohanty, R. K., & Das, M. (2009). Rainwater Management for Smallholder Irrigation and its Impact on Crop Yields in Eastern India. *Water Resources*

Management, *23*(7), 1237–1255. https://doi.org/10.1007/s11269-008-9324-y

St. Clair, J., Moon, S., Holbrook, W. S., Perron, J. T., Riebe, C. S., Martel, S. J., … Richter, D. d. (2015). Geophysical imaging reveals topographic stress control of bedrock weathering. *Science*, *350*(6260), 534–538. https://doi.org/10.1126/science.aab2210

Sukhija, B. S., Reddy, D. V., Nagabhushanam, P., & Hussain, S. (2003). Recharge processes: piston flow vs preferential flow in semi-arid aquifers of India. *Hydrogeology Journal*, *11*(3), 387–395. https://doi.org/10.1007/s10040-002-0243-3

UNESCO. (1999). *Water resources of hard rock aquifers in arid and semi-arid zones*. (J. W. Lloyd, Ed.). Paris, France: United Nations.

Ward, J., & Dillon, P. J. (2012). Principles to coordinate managed aquifer recharge with natural resource management policies in Australia. *HYDROGEOLOGY JOURNAL*, *20*(5), 943–956. https://doi.org/10.1007/s10040-012-0865-z

Warner, J. W., Molden, D., Chehata, M., & Sunada, D. K. (1989). Mathematical analysis of artificial recharge from basins. *Journal of the American Water Resources Association*, *25*(2), 401–411. https://doi.org/10.1111/j.1752-1688.1989.tb03077.x

Zhou, Y. (2009). A critical review of groundwater budget myth, safe yield and sustainability. *Journal of Hydrology*, *370*(1–4), 207–213. https://doi.org/10.1016/j.jhydrol.2009.03.009

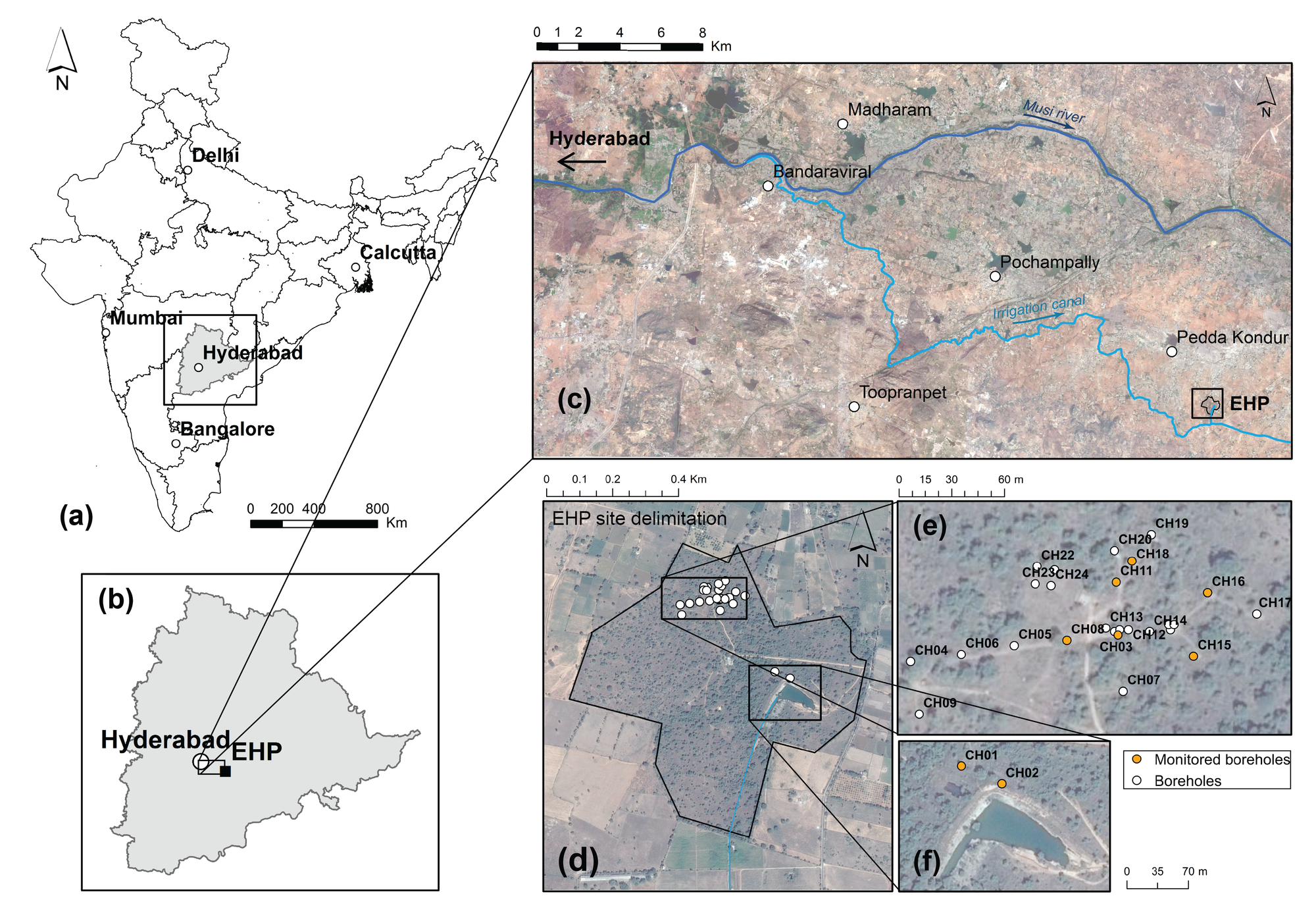
N
Delhi
Calcutta
Mumbai
Hyderabad
Bangalore
(a)
0 200 400 800 Km
(b)
Hyderabad
EHP
0 1 2 4 6 8 Km
Hyderabad
Madharam
Musi river
Bandaraviral
Pochampally
Irrigation canal
Pedda Kondur
Toopranpet
EHP
(c)
0 0.1 0.2 0.4 Km
EHP site delimitation
(d)
0 15 30 60 m
(e)
CH19
CH20
CH22
CH18
CH23
CH24
CH11
CH16
CH17
CH13
CH14
CH08
CH12
CH05
CH06
CH04
CH03
CH15
CH07
CH09
CH01
CH02
(f)
Monitored boreholes
Boreholes
0 35 70 m

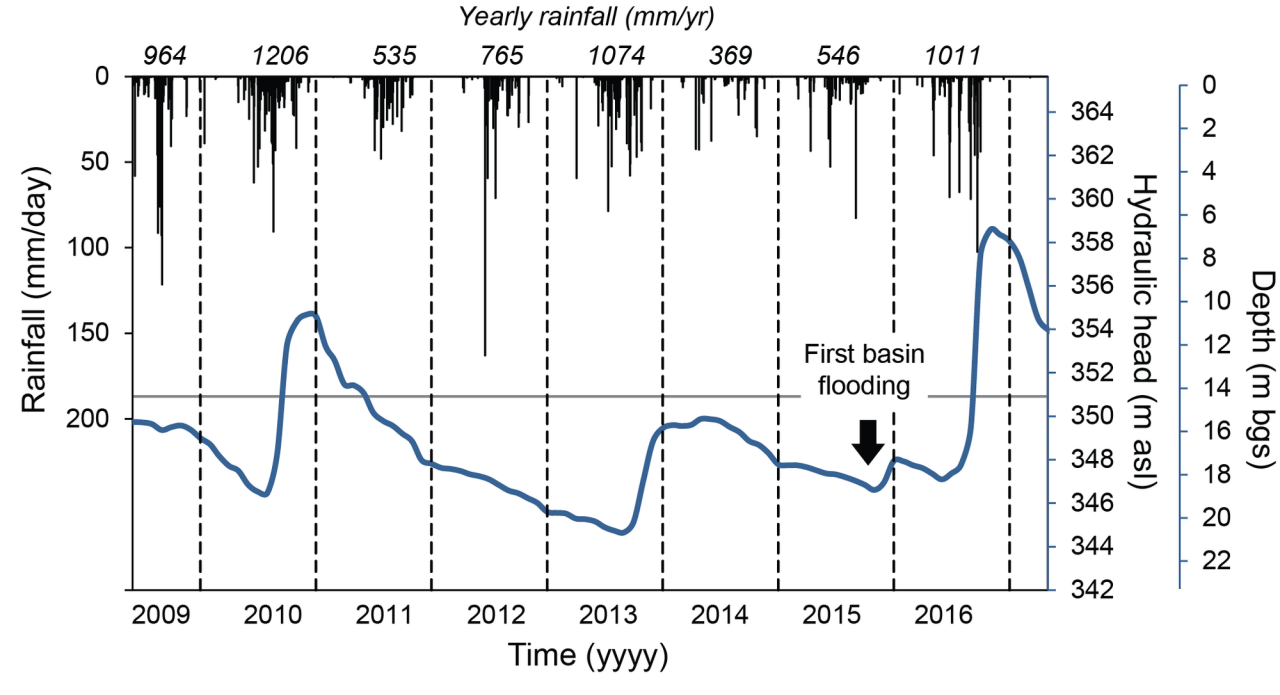
Yearly rainfall (mm/yr)
964
1206
535
765
1074
369
546
1011
Rainfall (mm/day)
0
50
100
150
200
Hydraulic head (m asl)
364
362
360
358
356
354
352
350
348
346
344
342
Depth (m bgs)
0
2
4
6
8
10
12
14
16
18
20
22
First basin flooding
2009
2010
2011
2012
2013
2014
2015
2016
Time (yyyy)

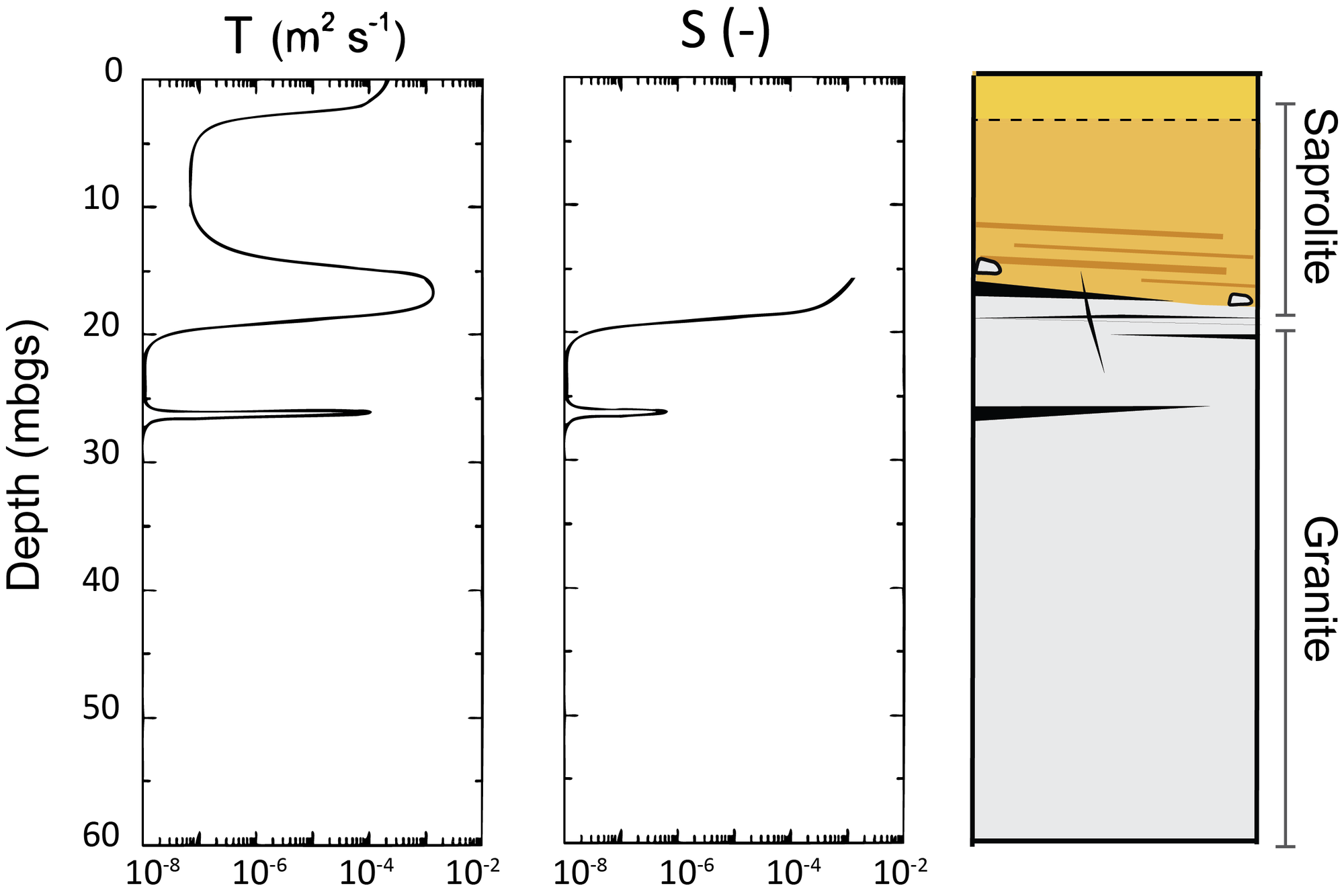
T (m² s⁻¹)
S (-)
Depth (mbgs)
0
10
20
30
40
50
60
10⁻⁸
10⁻⁶
10⁻⁴
10⁻²
10⁻⁸
10⁻⁶
10⁻⁴
10⁻²
Saprolite
Granite

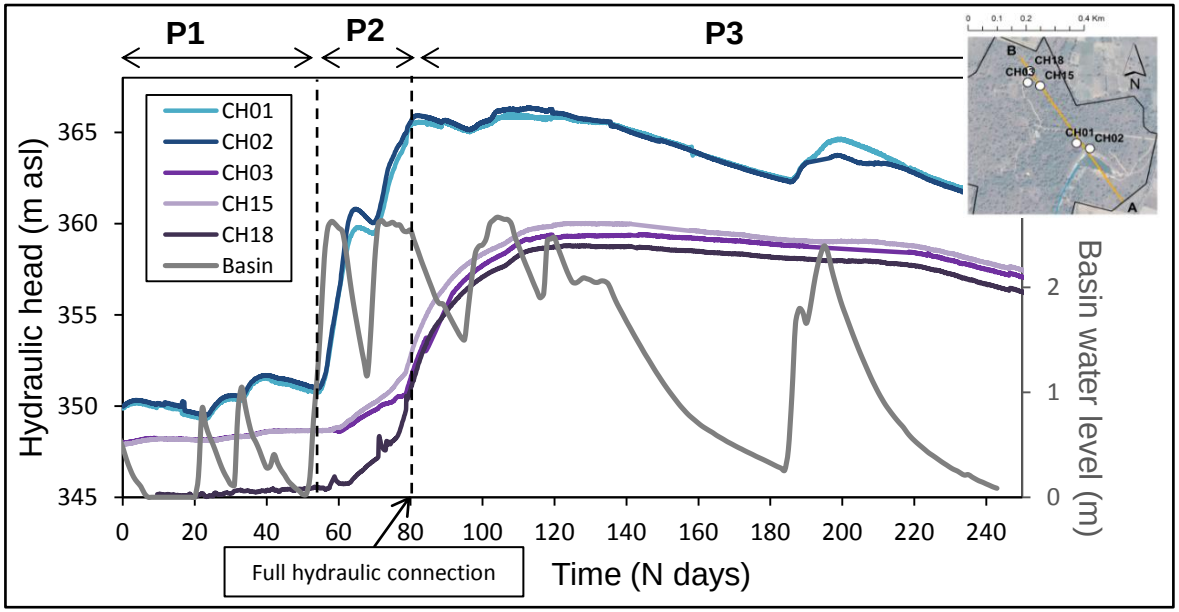
P1
P2
P3
CH01
CH02
CH03
CH15
CH18
Basin
Hydraulic head (m asl)
365
360
355
350
345
0
20
40
60
80
100
120
140
160
180
200
220
240
Time (N days)
Full hydraulic connection
Basin water level (m)
2
1
0
0 0.1 0.2 0.4 Km
B
CH18
CH03
CH15
N
CH01
CH02
A

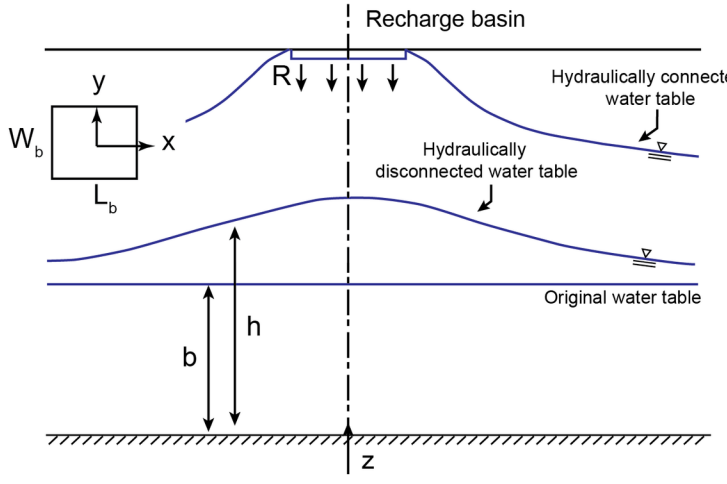

h = Water table elevation above the base of the aquifer (L)

b = Original saturated thickness (L)

$\overline{b}$ = Average saturated thickness (L)

L_b = Length of rectangular recharge basin (L)

W_b = Width of rectangular recharge basin (L)

R = Recharge rate (L/T)

K = Horizontal hydraulic conductivity (L/T)

S = Storage coefficient (dimensionless)

x, y = Cartesian coordinates with center of recharge basin as origin (L)

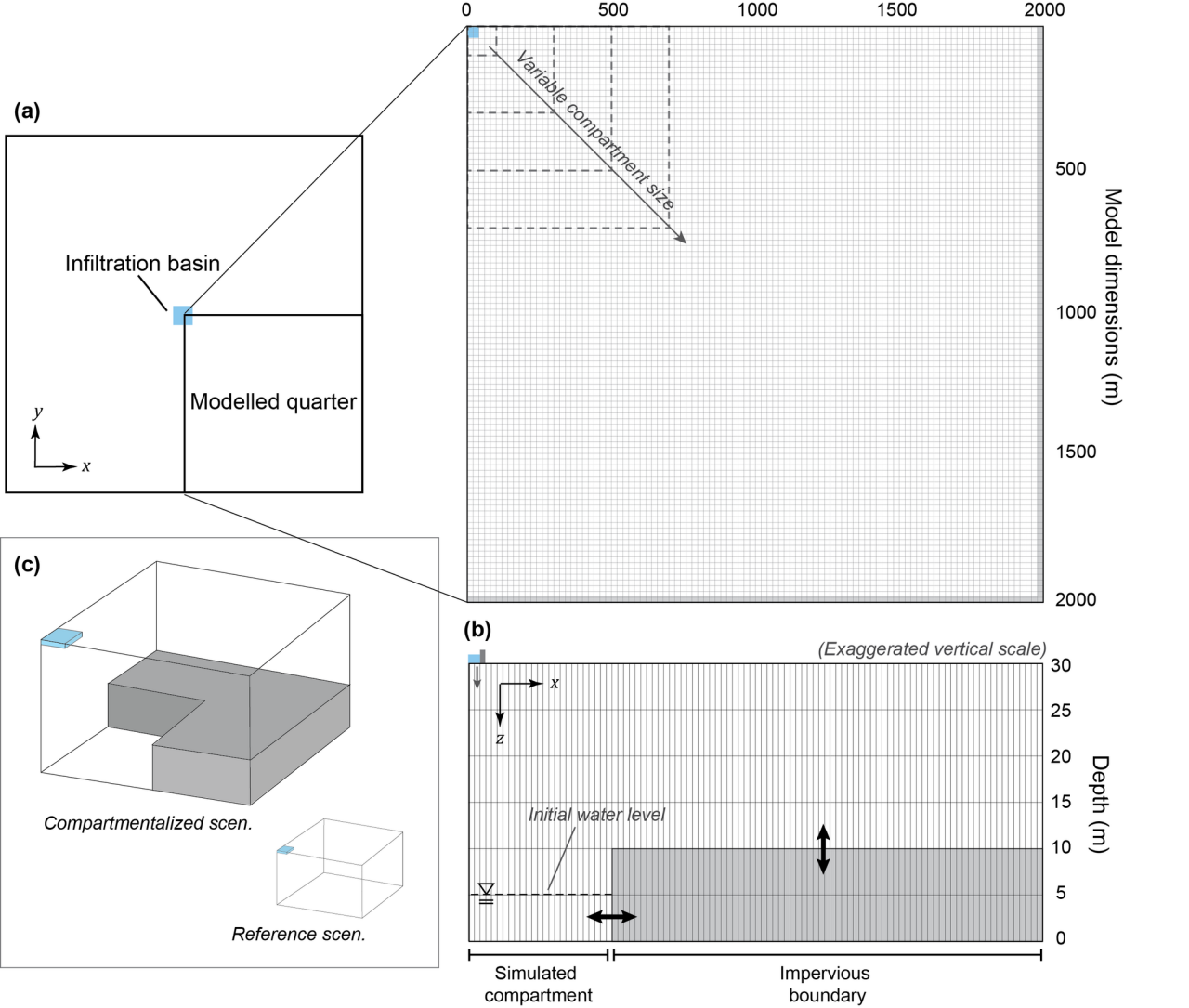
(a)
Infiltration basin
Modelled quarter
y
x
0
500
1000
1500
2000
Variable compartment size
Model dimensions (m)
(b)
(Exaggerated vertical scale)
x
z
Initial water level
Depth (m)
30
25
20
15
10
5
0
Simulated compartment
Impervious boundary
(c)
Compartmentalized scen.
Reference scen.

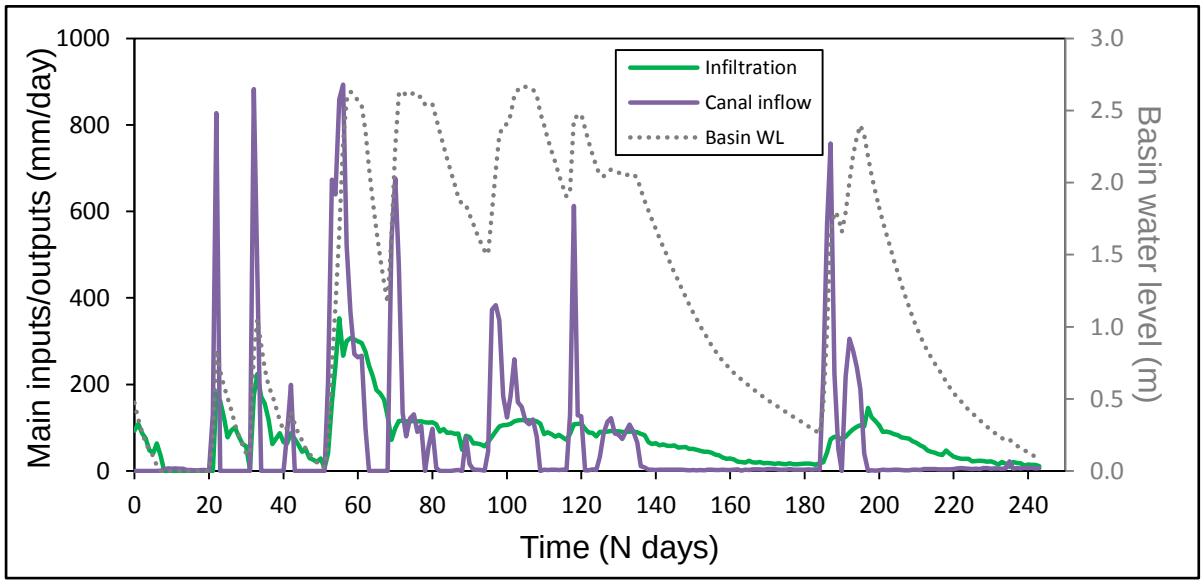
Main inputs/outputs (mm/day)
Basin water level (m)
Time (N days)
Infiltration
Canal inflow
Basin WL
1000
800
600
400
200
0
3.0
2.5
2.0
1.5
1.0
0.5
0.0
0
20
40
60
80
100
120
140
160
180
200
220
240

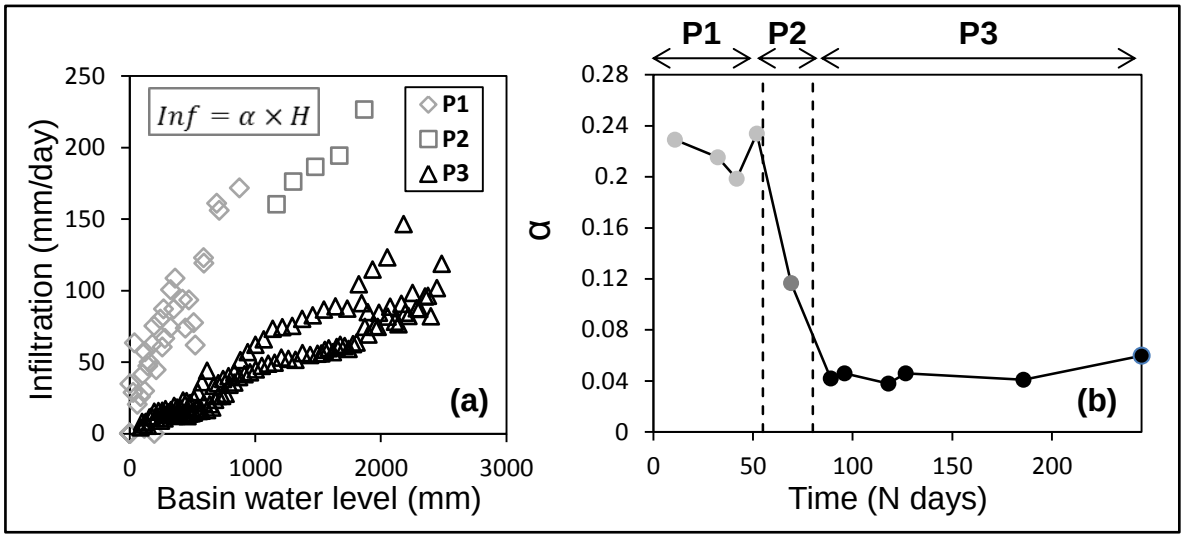
$Inf = \alpha \times H$
P1
P2
P3
Infiltration (mm/day)
Basin water level (mm)
(a)
P1
P2
P3
α
Time (N days)
(b)

0	0.28
55	55
80	80

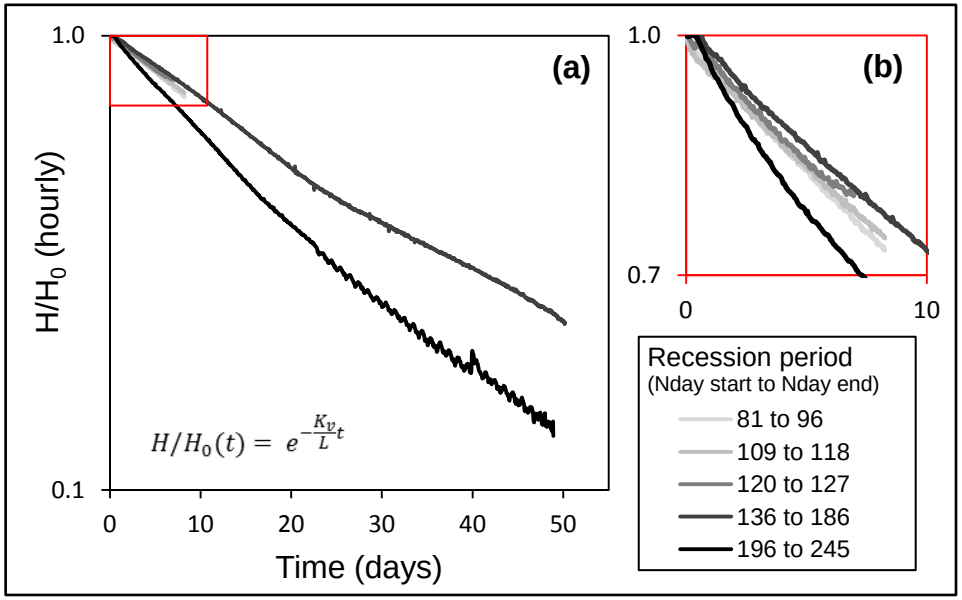
1.0
0.1
(a)
H/H0 (hourly)
$H/H_0(t) = e^{-\frac{K_y}{L}t}$
0
10
20
30
40
50
Time (days)
1.0
0.7
(b)
0
10
Recession period
(Nday start to Nday end)
81 to 96
109 to 118
120 to 127
136 to 186
196 to 245

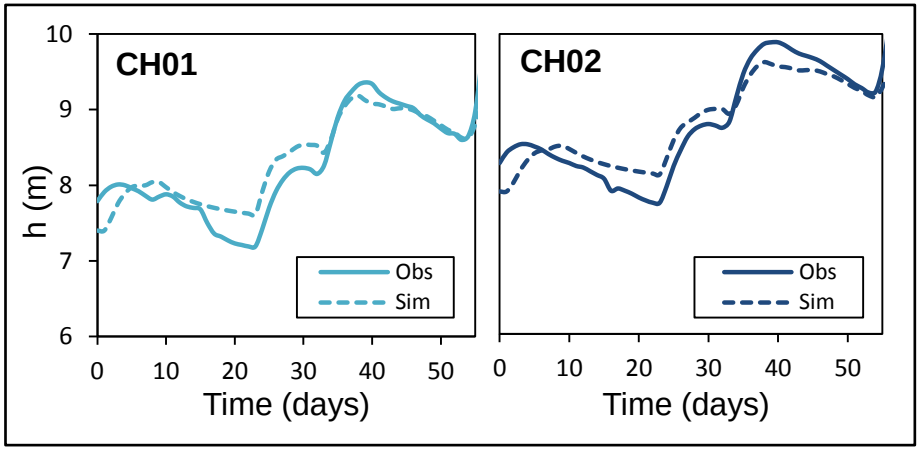
CH01
CH02
h (m)
10
9
8
7
6
0
10
20
30
40
50
Time (days)
Obs
Sim

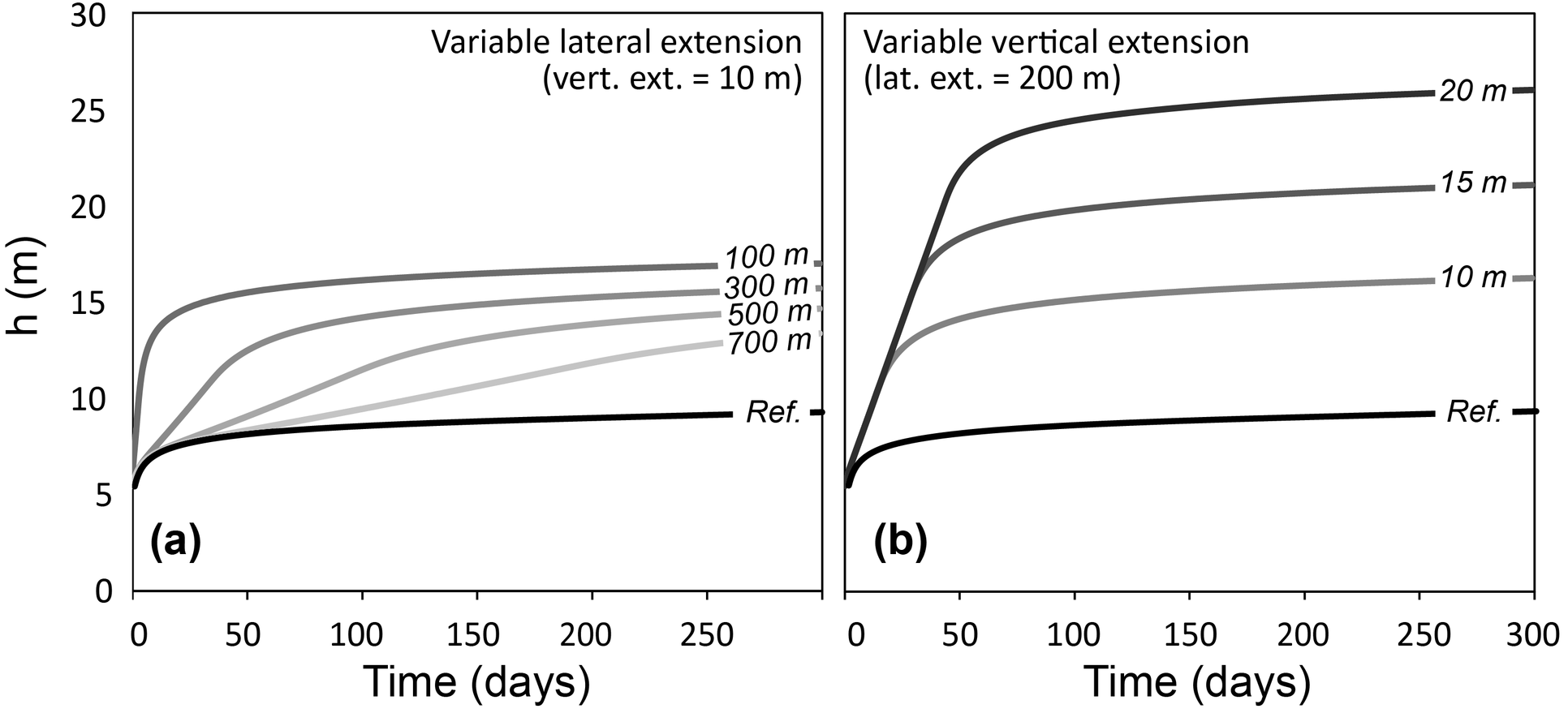
Variable lateral extension
(vert. ext. = 10 m)
100 m
300 m
500 m
700 m
Ref.
(a)
Variable vertical extension
(lat. ext. = 200 m)
20 m
15 m
10 m
Ref.
(b)
h (m)
0
5
10
15
20
25
30
0
50
100
150
200
250
300
Time (days)
Time (days)

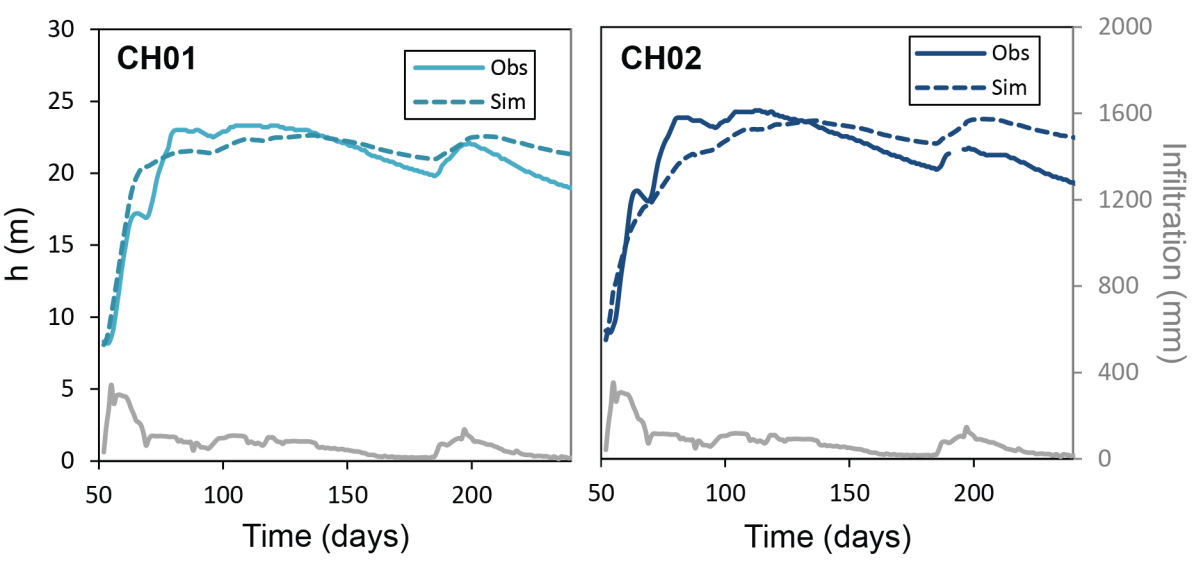
CH01
Obs
Sim
h (m)
30
25
20
15
10
5
0
50
100
150
200
Time (days)
CH02
Obs
Sim
2000
1600
1200
800
400
0
Infiltration (mm)
50
100
150
200
Time (days)

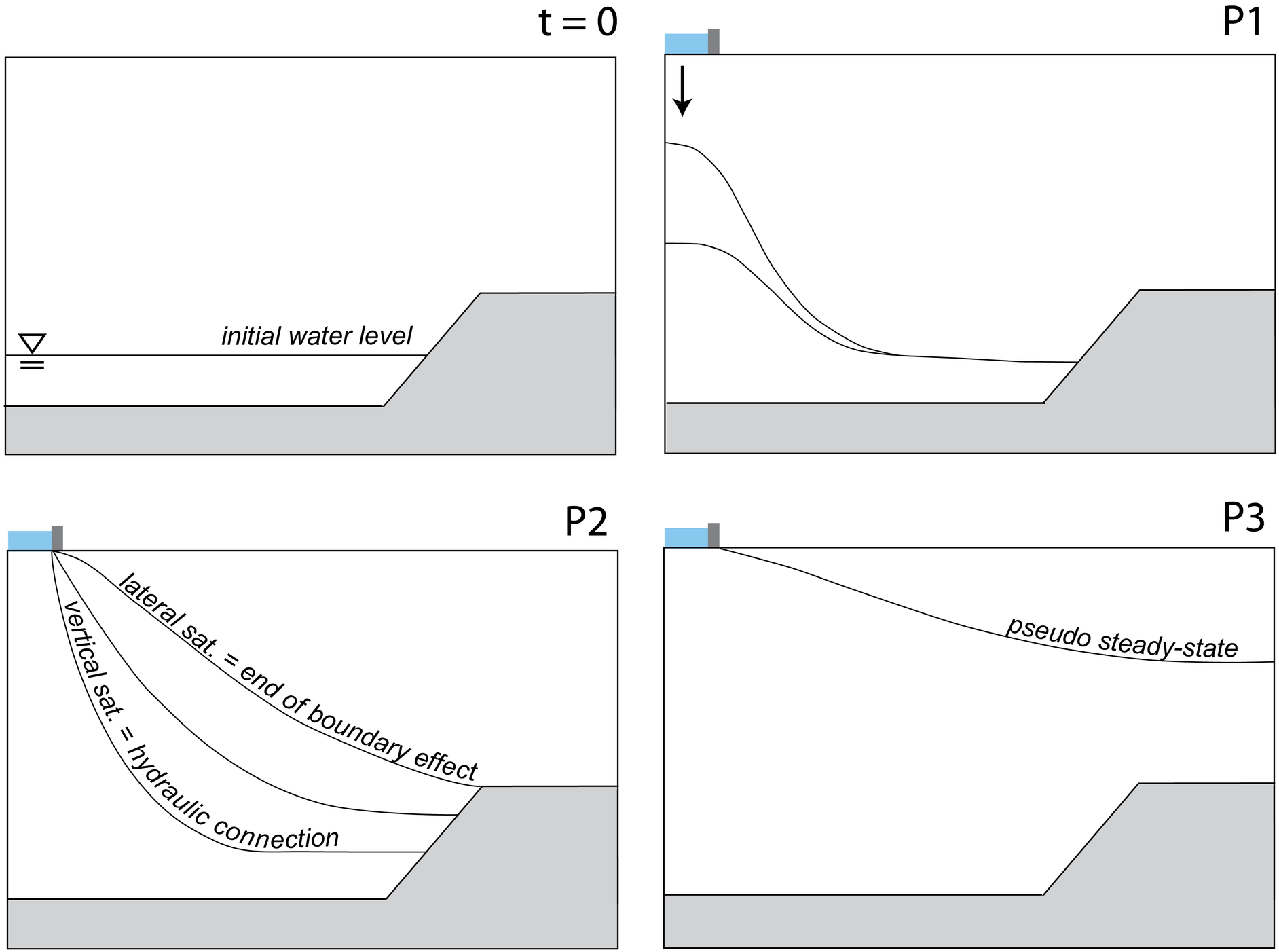
t = 0
initial water level
P1
P2
lateral sat. = end of boundary effect
vertical sat. = hydraulic connection
P3
pseudo steady-state

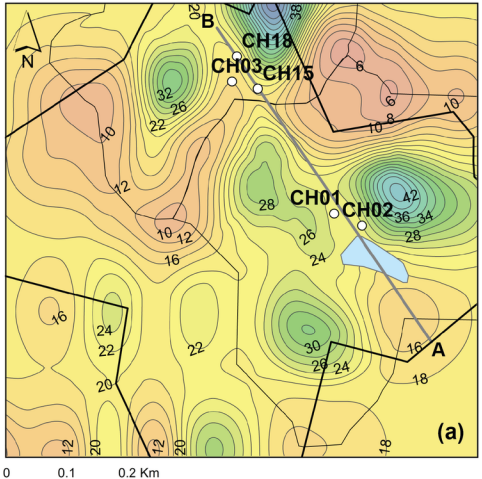

Interface relief depth (m bgs)

<4	28 - 30
4 - 6	30 - 32
6 - 8	32 - 34
8 - 10	34 - 36
10 - 12	36 - 38
12 - 14	38 - 40
14 - 16	40 - 42
16 - 18	42 - 44
18 - 20	44 - 46
20 - 22	46 - 48
22 - 24	48 - 50
24 - 26	50 - 52
26 - 28	

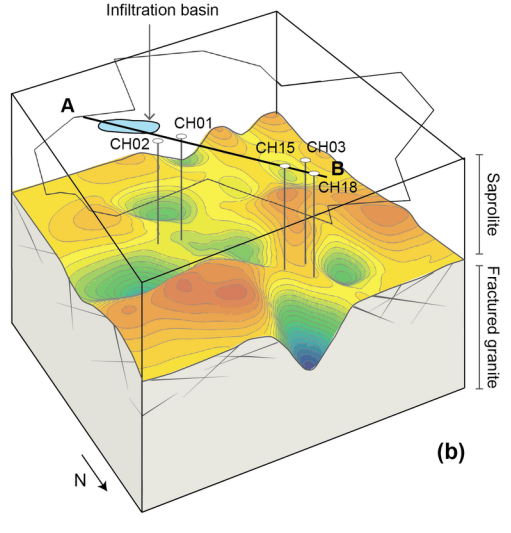

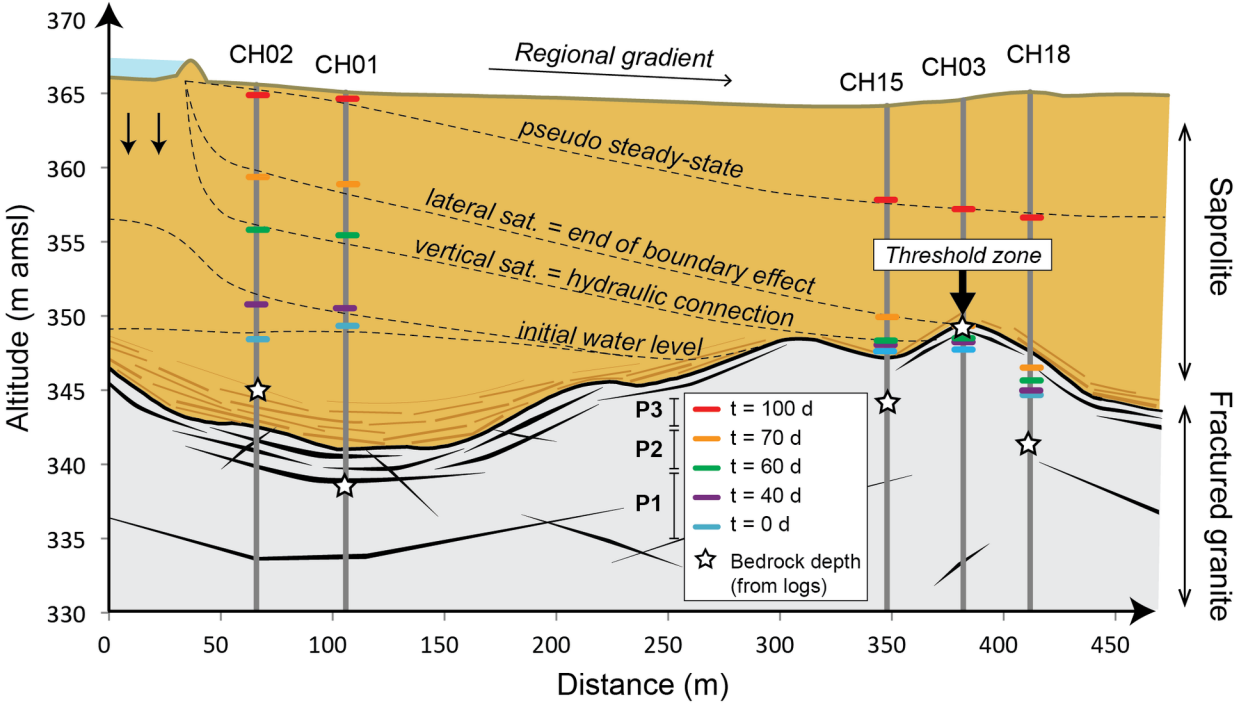
CH02
CH01
Regional gradient
CH15
CH03
CH18
pseudo steady-state
lateral sat. = end of boundary effect
vertical sat. = hydraulic connection
initial water level
Threshold zone
Saprolite
Fractured granite
P3
P2
P1
t = 100 d
t = 70 d
t = 60 d
t = 40 d
t = 0 d
Bedrock depth (from logs)
Altitude (m amsl)
Distance (m)
370
365
360
355
350
345
340
335
330
0
50
100
150
200
250
300
350
400
450

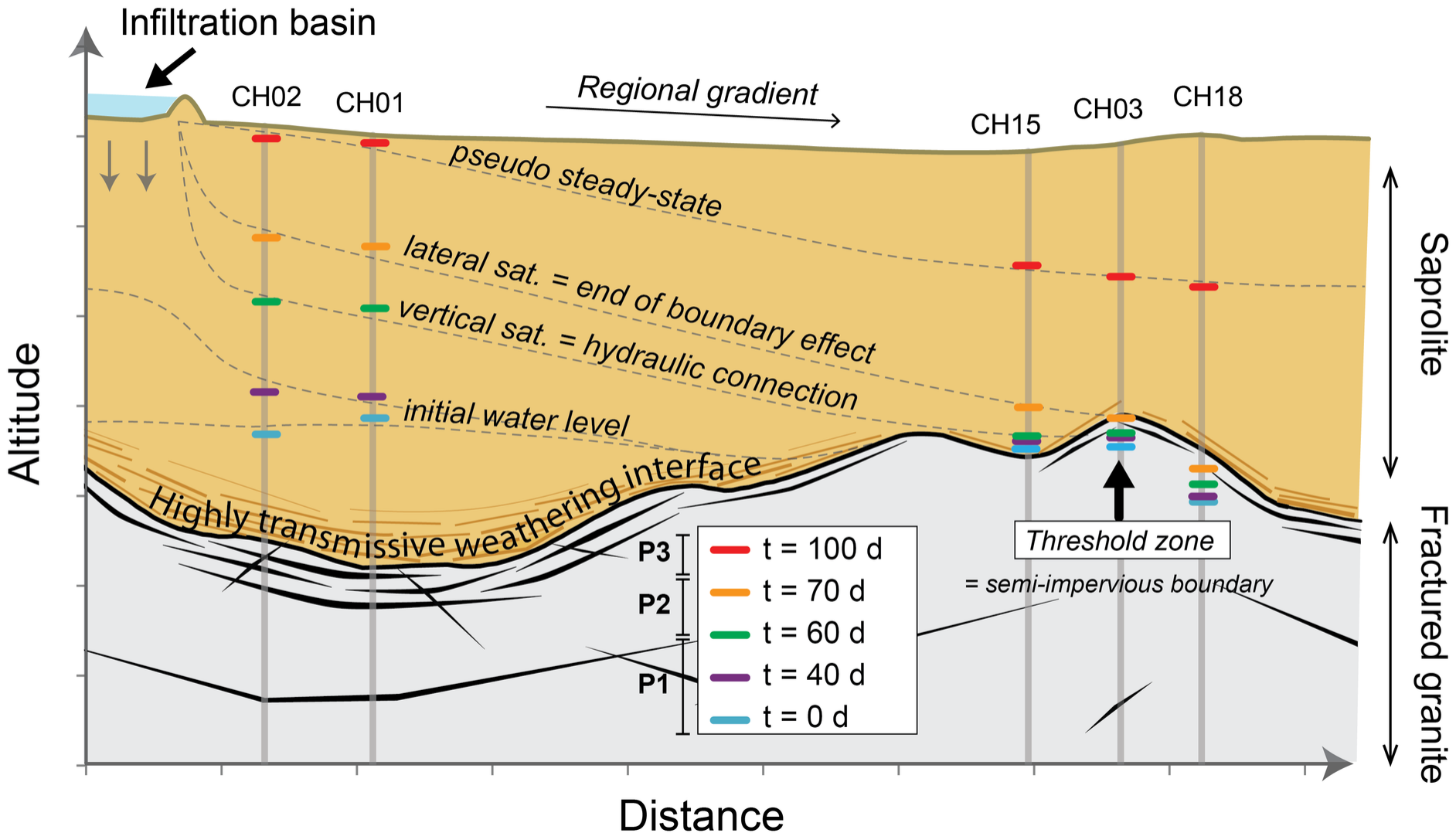
Infiltration basin
CH02
CH01
Regional gradient
CH15
CH03
CH18
pseudo steady-state
lateral sat. = end of boundary effect
vertical sat. = hydraulic connection
initial water level
Highly transmissive weathering interface
Saprolite
Fractured granite
Altitude
Distance
P3
P2
P1
t = 100 d
t = 70 d
t = 60 d
t = 40 d
t = 0 d
Threshold zone
= semi-impervious boundary